

Texas A&M University  
Mechanical Engineering Department  
Turbomachinery laboratory

**Dynamic Performance of a Squeeze  
Film Damper with Non-Circular  
Motions: Multiple-Frequency  
Reproducing Multi-Spool Engine  
Operating Conditions**

Research Progress Report to the Turbomachinery Research Consortium

**TRC-SFD-1-08**

**Adolfo Delgado**  
Research Assistant

**Luis San Andrés**  
Mast-Childs Professor  
Principal Investigator

June 2008

**TEES Project 32513/1519C3**

## Executive Summary

### TRC-SFD-1-08

Dynamic Performance of a Squeeze Film Damper with Non-Circular, Multi-Frequency Motions  
Reproducing Multi-Spool Engine Operating Conditions

Squeeze film dampers (SFDs) in rotating machinery provide structural isolation, reduce amplitudes of response to imbalance, and increase the threshold speed of rotor-bearing system instability. SFDs are usually installed at the bearing supports, either in series or in parallel. In multi-spool engines, SFDs are also located in the interface between rotating shafts. These *intershaft dampers* show multiple frequency whirl motions resulting from the combined imbalance responses of both the low speed rotor and the high speed rotor.

The report presents an experimental investigation simulating the dynamic forced response of a SFD subject to multiple frequency motions, as in a jet engine intershaft damper. For these operating condition, the forced response of the damper is non linear since its mechanical parameters, damping and inertia, are a function of the instantaneous journal position, static or dynamic.

The TRC-SFD test rig comprises of a vertical (stationary) journal and a flexibly supported housing that holds the test damper and instrumentation. The open ends SFD is 127 mm in diameter, 25.4 mm film land length, and radial clearance of 0.127 mm. The damper is lubricated with an ISO VG 2 oil and operated at room temperature (24 °C, feed pressure 24 kPa). In the experiments, two orthogonally positioned shakers are programmed to deliver dynamic forces to the test damper that produce certain controlled amplitude motions and, by using multi-frequency sine sweep excitations, to cover a frequency response range that includes the natural frequency of the test system. In the tests, a low frequency is maintained at 25 Hz, while a second frequency ramps from 30 Hz to 120 Hz over a specified time span. The test data collected, forces and motions versus time, is converted into the frequency domain for parameter identification, The SFD force coefficients are identified from system impedance functions and considering only the frequency component that coincides with the forced excitation frequency, since this is the only component that dissipates mechanical energy. The frequency dependent, identified viscous damping coefficients are strong functions of the amplitude of journal motion. In the tests, the damper operates free of oil cavitation or air entrainment, and

hence, the identified cross-coupled coefficients are negligible. The experimental added mass coefficients are three times larger than those predicted by classical theory, which ignores the influence of the inlet and discharge annular grooves. On the other hand, an improved bulk-flow model developed earlier (TRC-SFD-2-07) predicts added mass coefficient within 15% of the experimental values. The experimental damping coefficients are within the range of predictions derived from classical formulas for circular centered orbits or small amplitude motions about an eccentric journal position.

Note: The P.I. edited this report four times, English and technical content, prior to its release to TRC members.

## Table of Contents

Executive Summary .....	2
List of Tables and Figures.....	5
Nomenclature.....	8
I Introduction .....	9
II Literature Review .....	9
III Test Rig Description .....	13
IV Experimental Procedure and Parameter identification .....	17
V Identified SFD Force Coefficients and Comparisons to Predictions .....	22
Multiple Sine Sweep Excitations with Fixed Load Amplitude ( $F_1$ & $F_2$ ).....	22
Sine Sweep Excitations with Varying Load Amplitude ( $F_1$ & $F_2$ ) .....	28
Sine Sweep Excitations with Rotating Load Vector $F_3$ .....	33
VI Conclusions.....	39
VII References .....	41
Appendices	
A. Identification of Structural Parameters (dry system tests)	
B. Cross-coupled Impedance Functions Identified From Multiple Frequency Sine Sweep Excitation with Constant Amplitude	

## List of Tables

Table 1 Test conditions for dynamic load tests (CCO). Lubricated SFD (ISO VG 2).....	17
Table 2 SFD inertia coefficients identified from non-circular centered orbit tests (frequency range 40-80 Hz) ( $K_{sx}= 860$ kN/m, $K_{sy}= 890$ kN/m).....	26
Table 3 SFD inertia coefficients identified from non-circular centered orbit tests (frequency range 40-80 Hz). Varying load amplitude .....	31
Table 4 Damping coefficients estimated from fixed (set) SFD amplitudes (varying load amplitude) tests .....	32
Table 5 SFD inertia coefficients identified from rotating load of constant amplitude rotating load with multiple frequency sine sweep excitation (frequency range 40-80 Hz).....	37
Table A 1 Structural stiffnesses of support from static load tests.....	43
Table A 2 Identified parameters from impact tests exerted on SFD test section (no lubricant).....	44
Table B 1 Identified cross-coupled coefficients from constant amplitude load & sine sweep excitation tests.....	47

## List of Figures

Figure 1 Schematic view of intershaft tested in Ref. [8] .....	10
Figure 2 Test rig for dynamic force measurements and flow visualization in a sealed end SFD .....	14
Figure 3 SFD assembly cross section view. Detail view of SFD land and oil flow path .	15
Figure 4 Open-end SFD assembly cut view .....	16
Figure 5 SFD housing reference coordinate system and location of sensors .....	16
Figure 6 Detail view of test squeeze film damper geometry (open end).....	18
Figure 7 Schematic view of the equivalent representation of the SFD with mechanical seal .....	18
Figure 8 Damping coefficient versus journal eccentricity for circular centered orbits and radial displacements about an off-centered position [18].....	21

Figure 9 Bearing displacements for three amplitude load magnitudes, force excitation vector $F_1$ . Multiple frequency excitation (constant 25 Hz + chirp 30-120Hz). Clearance circle noted.....	23
Figure 10 Bearing displacements for three amplitude load magnitudes, force excitation vector $F_2$ . Multiple frequency excitation (constant 25 Hz + chirp 30-120Hz). Clearance circle noted) .....	24
Figure 11 $X, Y$ Forces and ensuing $X, Y$ displacements versus time. Excitation vector $F_1$ . Multiple-frequency excitation (constant 25Hz + sine sweep 30-120Hz). (Maximum motion amplitude $\sim 60 \mu\text{m}$ ) .....	24
Figure 12 FFT of input forces and ensuing displacements $X, Y$ due to excitation vector $F_1$ .....	25
Figure 13 Real part of direct impedances versus frequency. Multiple frequency excitation (constant 25Hz + sine sweep 30-120Hz). ( $K_{sx}= 860 \text{ kN/m}$ , $K_{sy}= 890 \text{ kN/m}$ ). Excitation vectors $F_1$ & $F_2$ .....	26
Figure 14 Imaginary part of direct impedances $\times (1/\omega)$ versus excitation frequency. Multiple frequency excitation (constant 25Hz + sine sweep 30-120Hz). Excitation vectors $F_1$ & $F_2$ .....	27
Figure 15 Direct squeeze film damping coefficients identified from fixed load amplitude, multiple frequency load excitations. (25Hz + sine sweep 30-120Hz). Excitation vectors $F_1$ & $F_2$ ). Predictions for circular centered orbits (CCO) and radial motion about an off-centered journal position .....	28
Figure 16 Excitation forces $F_x, F_y$ and ensuing $X, Y$ bearing displacements versus time (Set maximum journal amplitude $\sim 15 \mu\text{m}$ ).....	29
Figure 17 Excitation forces $F_x, F_y$ and ensuing $X, Y$ bearing displacements versus time (Set maximum journal amplitude $\sim 30 \mu\text{m}$ ).....	29
Figure 18 Excitation forces $F_x, F_y$ and ensuing $X, Y$ bearing displacements versus time (Set maximum journal amplitude $\sim 50 \mu\text{m}$ ).....	30
Figure 19 Frequency spectra of $X$ -force and ensuing $X$ -displacement. Time data shown in Figures 16-18 .....	30
Figure 20 Imaginary part of impedance functions, $\text{Im}(F_x/X)$ & $\text{Im}(F_y/Y)$ . Non-circular orbits, multiple frequency load excitations. Maximum displacement amplitudes: 15 $\mu\text{m}$ and 50 $\mu\text{m}$ .....	32

Figure 21 Direct squeeze film damping coefficients identified from varying load amplitude, multiple frequency load excitations. (25Hz + sine sweep 30-120Hz). Predictions for circular centered orbits (CCO) and radial motion about an off-centered journal position.....	33
Figure 22 Excitation forces $F_x$ , $F_y$ and ensuing $X$ , $Y$ bearing displacements versus time. Excitation vector $F_3$ : rotating load, sine sweep frequency.....	34
Figure 23 Frequency spectra of $X$ & $Y$ forces and ensuing $X$ & $Y$ displacements. Time data shown in Figure 22. rotating load vector $F_3$ .....	35
Figure 24 Recorded bearing orbits due to rotating load vector $F_3$ . Motions shown for time intervals $0-1/4\tau$ , $0-1/2\tau$ , $0-3/4\tau$ , $0-1\tau$ . Multi-frequency excitation (constant 25 Hz + sine sweep 30-120Hz). Clearance circle noted. ....	36
Figure 25 Real part of direct impedances versus frequency. Constant amplitude rotating load with multiple frequency sine sweep excitation ( $K_{sx}= 860$ kN/m, $K_{sy}= 890$ kN/m) .....	37
Figure 26 Imaginary part of direct impedances $\times (1/\omega)$ versus frequency. Constant amplitude rotating load with multiple frequency sine sweep excitation.....	38
Figure 27 Direct squeeze film damping coefficients identified from constant amplitude rotating load with multiple frequency sine sweep excitations (Excitation vector $F_3$ ). Predictions for circular centered orbits (CCO) and radial motion about an off-centered journal position.....	39
Figure A 1 Bearing deflection versus static load ( $X, Y$ directions).....	43
Figure A 2 Impact load and displacements ( $X, Y$ ) versus time (dry system).....	44
Figure A 3 Transfer function ( $X/F_x$ ) from impact load tests and curve fit for motions along $X$ direction. (Dry system, no seal).....	45
Figure A 4 Transfer function ( $Y/F_y$ ) from impact load tests and curve fit for motions along $Y$ direction. (Dry system, no seal).....	45
Figure B 1 Real part of cross-coupled impedance function. Non-circular orbit, constant amplitude sine sweep excitation load.....	46
Figure B 2 Imaginary part of cross-coupled impedance function. Non-circular orbit, constant amplitude chirp excitation load .....	47

## Nomenclature

$c$	Bearing radial clearance [m]
$C_{rv}$	Structure remnant damping coefficient [N.s/m]
$C_{s\alpha}$	Structure damping coefficient [N.s/m] $\alpha=x,y$
$C_{s-\alpha\beta}$	Identified system damping coefficients [N.s/m] $\alpha,\beta=x,y$
$C_{SFD\alpha\beta}$	Identified squeeze film damping coefficients [N.s/m] $\alpha,\beta=x,y$
$D$	2 $R$ . Damper journal diameter [m]
$e$	Amplitude or radius of circular centered orbit [m]
$F_{x,y}$	External (shaker) forces applied to bearing [N]
$\bar{F}_x, \bar{F}_y$	Complex components of external forces applied to bearing [N]
$F_d$	Dry friction force from contact in mechanical seal [N]
$f_n$	Test system natural frequency [Hz]
$H_{\alpha\beta}$	Dynamic transfer functions [N/m], $\alpha,\beta=x,y$
$K_{sx}, K_{sy}$	Structural (support) stiffnesses [N/m]
$L, R$	Length and radius of SFD land [m]
$M_s$	Mass of SFD housing [kg]
$M_f$	Estimated mass of lubricant (feed plenum & end groove) [kg]
$M_{SFD\alpha\beta}$	Squeeze film inertia coefficients [kg], $\alpha,\beta=x,y$
$M_{s-\alpha\beta}$	Identified system inertia coefficients [kg], $\alpha,\beta=x,y$
$M_{plenum}$	Oil mass at the SFD inlet plenum [kg]
$T$	Lubricant temperature [°C]
$x,y$	Bearing dynamic motions along $X,Y$ directions [m]
$\bar{x}, \bar{y}$	Complex components of bearing motions [m]
$\dot{x}, \dot{y}$	Bearing dynamic velocities along $X,Y$ directions
$Z(\omega)$	Vector of displacements in frequency domain [m]
$\rho, \eta$	Lubricant density [ $\text{kg/m}^3$ ] and viscosity [Pa-s]
$\tau$	Sampling period of excitation signal [sec]
$\omega$	Excitation frequency [rad/s]

## I Introduction

Squeeze film dampers provide structural isolation, reduce imbalance response amplitude levels in rotating machinery, and in some instances, increase the rotor speed stability threshold. SFDs are typically found in aircraft engines and also in land base rotating equipment. SFDs are usually installed at the bearing supports, either in series or in parallel. In the case of multi-spool engines, SFDs can also be located in the interface between rotating shafts (see Fig. 1). These dampers, known as *intershaft dampers* (ISDs), are subject to whirl motions resulting from the combined imbalance response of both the low speed and the high speed rotors. The resulting motions are non-circular and with multiple frequency components.

The present work aims to investigate the dynamic response of a SFD subject to multiple frequency whirling motions, similar to those found in the operation of an intershaft SFD in a jet engine. For such motions, the forced response of the damper is apparently nonlinear since the SFD force coefficients are a function of the instantaneous motion amplitude.

Presently, damping coefficients are identified from multiple frequency sine sweep force excitations over a frequency range that includes the natural frequency of the test system. Prior reports [1-4] describe the test rig for experimentation on a SFD with a contacting mechanical end seal. Currently, the mechanical end seal is not active, and the oil is free to exit the damper at the discharge end. A review of prior relevant work to this research and a description of the test rig follow.

## II Literature Review

This review includes publications related to intershaft dampers (ISDs) and identification of SFD force coefficients from non-circular orbits. In the late 1970's, Hibner [5] presents an analysis to predict the dynamic response of a multi-shaft gas turbine engine with an ISD. The analysis provides natural frequency maps and deflection modes of the two shafts for two different speed ratios between the low speed rotor and high speed rotor (2X and 3X). Engine operation is simulated with different levels of imbalance for both shafts, and the amplitude response of the machine housing is presented for two cases, with and without ISD. Hibner indicates that the typical speed ratio (high speed shaft/ low speed shaft) is between 4 and 2 (any fraction) for this type of

damper. The author also shows the importance on the dynamic response due to the interaction of the rotor vibration modes and the resulting relative motions at the damper location.

Hibner *et al.* [6,7] present an analytical and experimental study of the dynamic performance of intershaft dampers in multi-spool gas turbines, and consider possible methods to tune the damper to avoid unstable operation. At the time, intershaft dampers did not include an anti-rotation pin, and thus the damper exhibited the same dynamic response as that of a large clearance plain journal bearing, which explains the unstable operation reported in Refs. [6,7].

Gupta *et al.* [8] test three ISD configurations including combinations of support springs (i.e. attached to the outer race of damper) and centralizing springs (i.e. attached to inner race of the damper) as shown in Fig. 1. Incidentally, the pressure profile sketched in the figure is most likely incorrect since it assumes a null dynamic pressure at the central feed groove (see Ref. [9]).

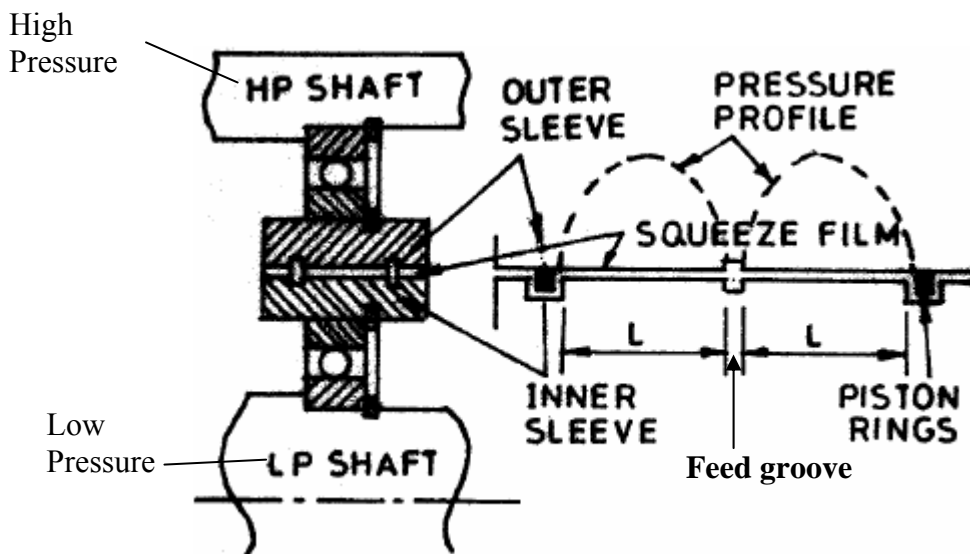


Figure 1 Schematic view of intershaft tested in Ref. [8]

The results in Ref. [8] reveal that the most favorable ISD configuration is the one with a centralizing spring. The authors present analytical expressions for the force coefficients integrated into a FE model of the rotor-bearing system to predict the system rotordynamic response. Based on predictions, the authors identify the optimum clearance for the damper. There is no experimental validation and the authors define a stiffness

associated to the squeeze film that is function of the whirl frequency. This is a pervasive incorrect assumption since squeeze films do not generate forces proportional to journal displacement but to journal velocity.

Chen *et al.* [10] present an analysis to predict the response of an ISD for the case where the high and low speed shafts describe synchronous offset elliptical orbits. The authors derive the pressure profile from a simplified Reynolds equation using the short bearing length model and obtaining linearized force coefficients from a harmonic balance procedure. The method is limited to operating conditions with a steady state response for the ideal case (i.e. synchronous vibration of both shafts).

The literature on parameter identification methods is extensive. In particular, the identification of force coefficient in SFDs has been extensively reported. However, most works deal with identification of force coefficients from circular orbits. Adilleta and Della Pietra [11,12] review most of the relevant analytical and experimental work conducted on SFDs up to 2002. San Andrés and Delgado [4] present a review of additional experimental works conducted from on SFDs from 2002 to date.

Tiwari *et al.* [13] provide a comprehensive review of the techniques used to characterize the mechanical parameters of fluid film bearings. The review includes different approaches for identifying force coefficients in all bearing types, including different input excitations, mathematical models, and uncertainty associated to the identification methods.

El-Shafei [14] presents a technique to estimate equivalent force coefficients best representing the dynamic response of a SFD describing elliptic orbits. The method relies on the least square minimization of the difference between the actual and equivalent linearized forced response of the test system. Linear force coefficients are obtained from the energy dissipated in terms of the respective system response (i.e. acceleration, velocity, displacement). The method is applied to estimate the imbalance response of a rotor mounted on two SFDs. The response orbits of the system are estimated using an iterative algorithm to identify the linear coefficients. The results compare well to numerical transient response simulations using SFD (nonlinear) impedances. El-Shafei uses various combinations of parameters (mass, stiffness and damping) to characterize the damper forced response. One of the models includes direct stiffnesses generated by the squeeze film while ignoring the added mass terms. This approach is not consistent

with prevailing literature [11,12], in which squeeze films do not generate forces proportional to journal (static) displacements and the added mass coefficients are not negligible.

Zhang and Roberts [15] present a method to identify force coefficients on a SFD executing both radial and circular motions about a centered position. The equations of motion and corresponding nonlinear parameters are presented for radial and circular motions, and a matrix of nonlinear response terms (following a power law form) is constructed. The coefficients of each response terms are obtained in the frequency domain by multiplying the inputs and outputs by windowing functions that allow correlating each of the nonlinear outputs to the input (using properties of the Fourier transform). The parameters are identified for pure radial motions using numerical integration of a SFD system excited with a force containing three single frequency signals. The identified SFD parameters show good correlation with similar parameters obtained from a numerical simulated response depending on the excitation frequencies selected (i.e. with or w/o including the natural frequency). The authors model the SFD damping force as a polynomial function of the journal displacement including odd and even coefficients. This representation is not physically correct. Using an odd polynomial terms yield a force that both follows and opposes the journal motion in a single period of motion. Thus, such force can not be dissipative. Furthermore, the authors characterize the response of the damper in terms of 10 force coefficients, which is rather impractical. The mayor limitation of this method lies on the requirements for the excitation signal. In addition, some of the non-linear inputs given on the equations of motion of the SFD are correlated, and this method cannot distinguish between the contributions of these inputs (i.e.  $x^2 * \dot{x}$  and  $\dot{x}$ )

Ellis *et al.* [16] experimentally identify the force coefficients of a SFD using a time-domain technique. The identification method is based on the instrumental variable filter (IVF) method and relies on solving an auxiliary system of differential equation to obtain the force parameters of the damper. The excitation force includes the sum of two sinusoidal signals at frequencies below and above the natural frequency of the system. The force coefficients are presented as a function of the operating clearance and compared to theoretical predictions. Although the authors use multiple frequency

excitations, the force coefficients are identified for centered and off-centered operation for small motion amplitudes to avoid non-linear effects.

Diaz and San Andrés [17] present two methods for identification of damping coefficients in a SFD. The first method consists on a least-squares curve fitting of the damping forces in the time domain, and the second one is based on approximating a measured rotor orbit with its synchronous components (Filtered Orbit Method). The frequency domain method proves to be more adequate and simpler than the time domain method. The results from the experiments show that the identified damping coefficients are insensitive to whirl frequency and nearly independent of the imbalance magnitude.

San Andrés and De Santiago [18] identify experimentally the damping and added mass coefficients of an open-end squeeze film damper for large elliptical and circular orbits. The force coefficients are obtained from single frequency excitations following an identification procedure frequency domain neglecting cross-coupled coefficients. The authors investigate the reduction of the film damping capabilities due to air entrapment. For the largest test journal orbits, the air entrapment is accounted for as a reduction of the effective length of the damper rather than a reduction in the effective viscosity of the fluid/air film mixture (as represented in previous analytical efforts). The effective length of the SFD is frequency and amplitude dependent, as the amount of air entrapped is a function of these two variables. In the experiments presented, the effective length ranged from 82% to 78% of the actual damper length. The identified damping force coefficients for small amplitude orbits agree well with predictions from classical theory [19], except for the identified inertia coefficients that are approximately twice as large as those obtained from predictions.

### III Test Rig Description

A prior TRC report [4] describes the main components of the test rig incorporating a SFD with a contacting (non rotating) mechanical seal. Presently, the wave spring loading the end seal is removed and the oil can leak through this end. Figure 2 depicts a schematic view of the test rig consisting of a vertical rigid shaft, mounted on three precision ball bearings (natural frequency 400 Hz [3]), which holds a steel journal of 5” (127 mm) diameter and 3” (76.2 mm) long. The bearing assembly includes two steel plates clamping an acrylic bearing. The two horizontal plates are attached by two vertical

steel plates, which also serve as an interface to apply external forces onto the bearing assembly. The top plate includes a lubricant supply connection, a static pressure gauge displaying the feed pressure into the bearing and four eddy current sensors facing the shaft. The composite bearing housing hangs from a top structure with four steel rods providing structural stiffness to the test bearing section. A mechanism atop of the test rig, comprising two sliding flat plates (top and bottom support plates), allows adjusting the position of the bearing center with respect to the shaft to simulate centered and off-centered operation conditions.

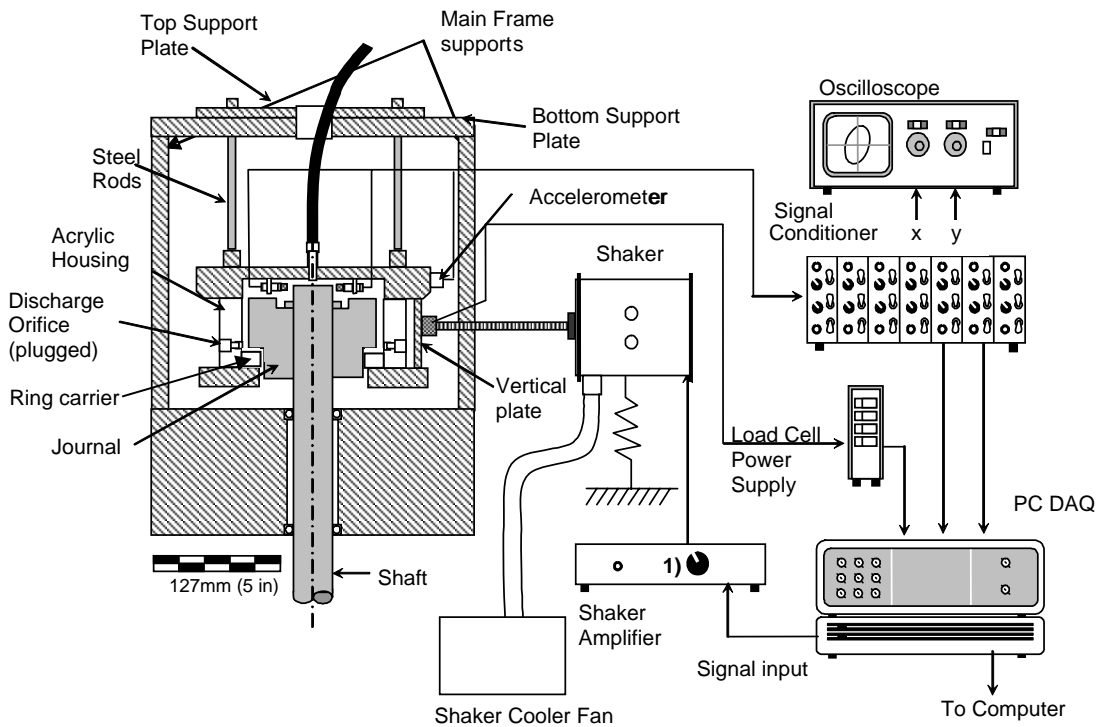


**Figure 2 Test rig for dynamic force measurements and flow visualization in a sealed end SFD**

The bearing housing design integrates a SFD land and inlet groove. Figure 3 and 4 depict a cross section and a cut view of the end sealed SFD design along with its components, respectively. Figure 4 shows the instrumentation arrangement and the reference coordinate system on the SFD housing. The instrumentation consists of two accelerometers, four eddy current sensors and two load cells. The system is excited via two electromagnetic shakers suspended from separate steel structures (90 degrees apart). Slender stingers connect the electromagnetic shakers to the piezoelectric load cells

attached to vertical plates on the bearing housing. A customized data acquisition system records all the sensor signals and controls the electromagnetic shakers.

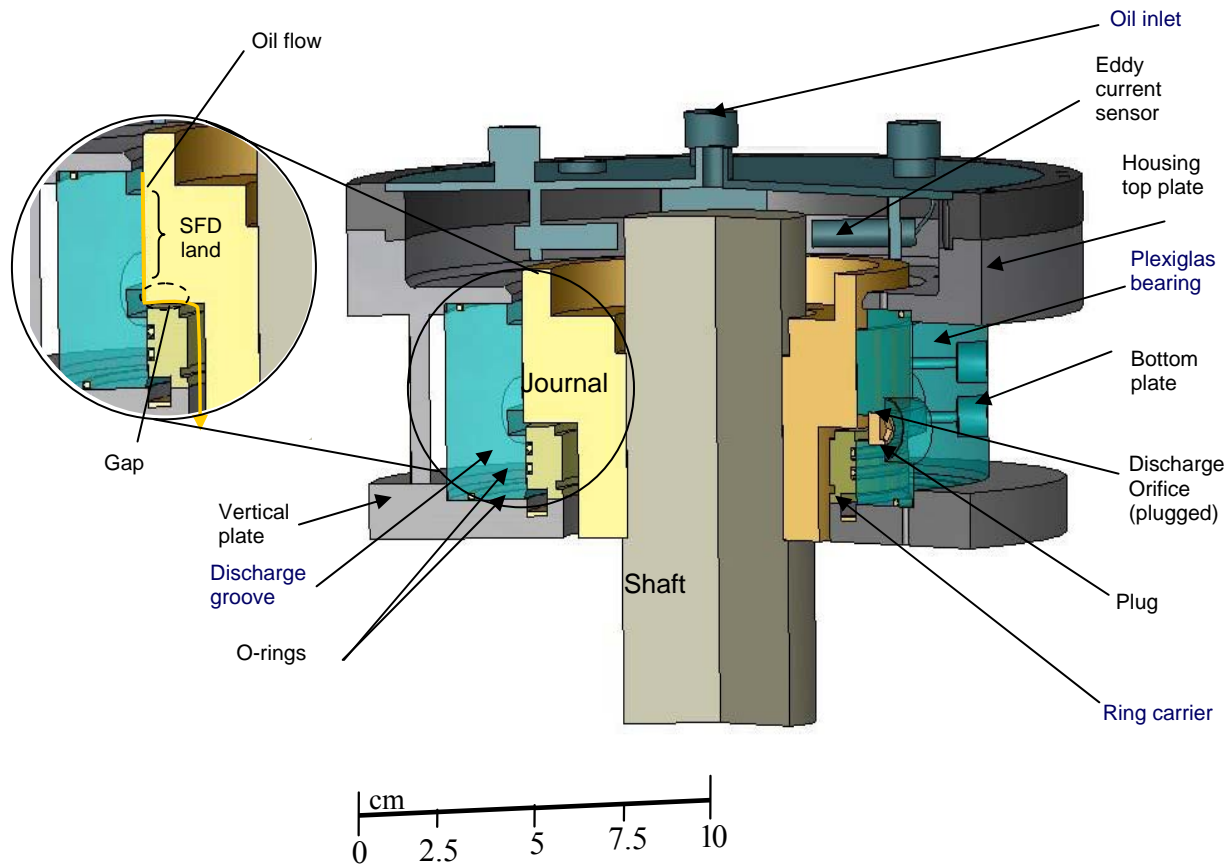


**Figure 3 SFD assembly cross section view. Detail view of SFD land and oil flow path**

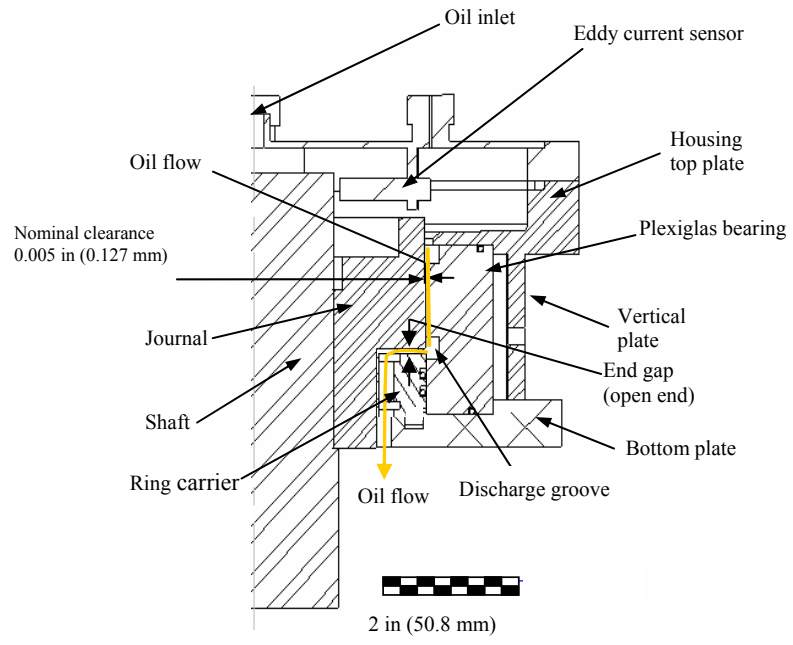


**Figure 4 Open-end SFD assembly cut view**

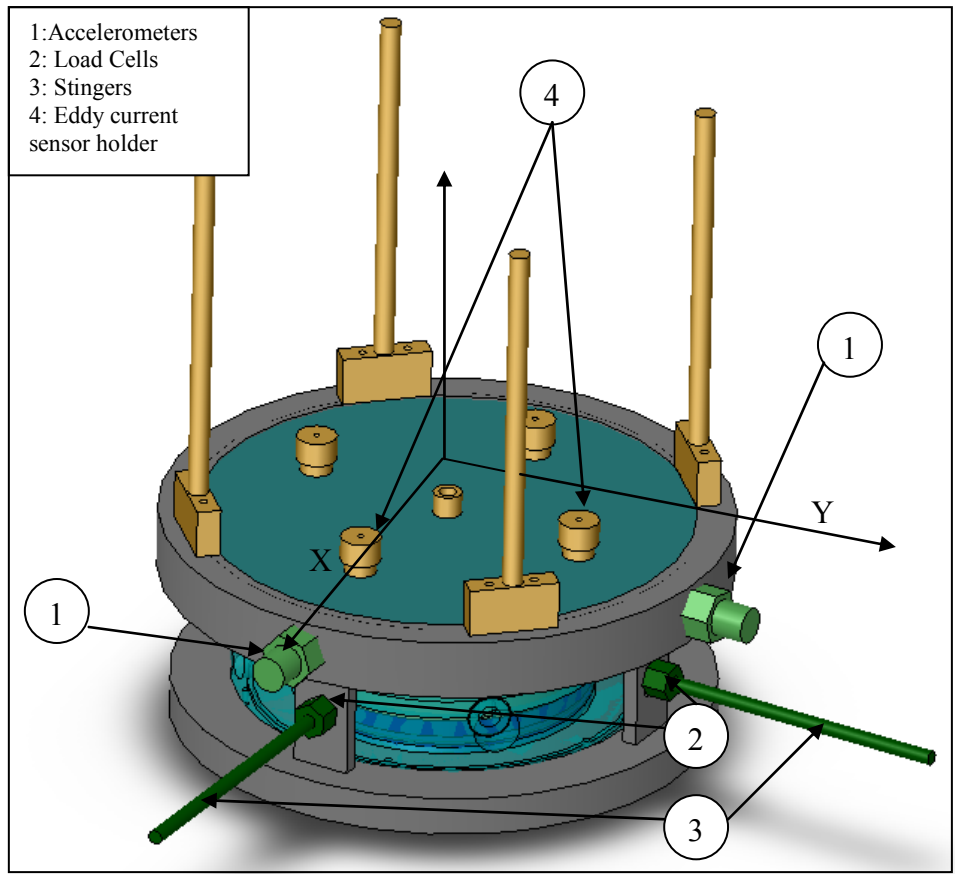


**Figure 5 SFD housing reference coordinate system and location of sensors**

## IV Experimental Procedure and Parameter identification

Two orthogonally mounted electromagnetic shakers excite the system with superimposed multiple frequencies to reproduce the operation of two cylinders whirling with different amplitudes and frequencies (i.e. an intershaft squeeze film damper). The excitation force includes the combination of a single frequency excitation (25 Hz) representing the low speed shaft and a varying sine sweep (or chirp) excitation (30 Hz to 120 Hz) representing the high speed shaft. In the tests, the SFD is excited with a combination of the following functions:

$$\begin{aligned} F_s(t) &= A \sin(2\pi f_0 t) + B \sin(2\pi f_1(t)t); \\ F_c(t) &= A \cos(2\pi f_0 t) + B \cos(2\pi f_1(t)t); \end{aligned} \quad (1)$$

where  $f_0$  (25 Hz) is the fixed frequency representing the low speed rotor whirling frequency, and

$$f_1(t) = (30 + 90t) \quad (2)$$

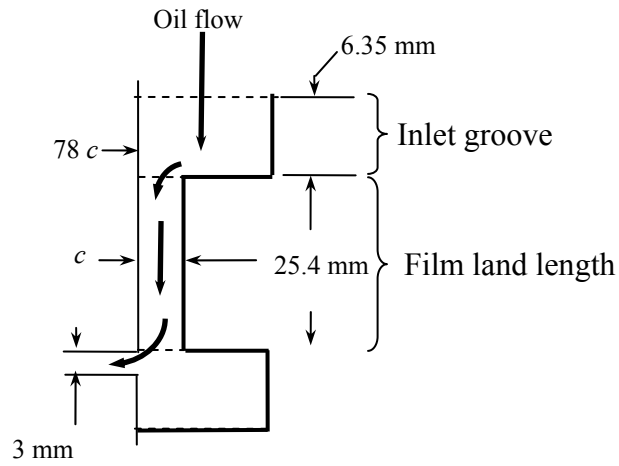
varies from 30 up to 120 Hz and represents the whirling frequency of the high speed rotor.  $A$ ,  $B$  are the amplitudes of the excitation load. The sine sweep excitations last one (1) second and the record sampling frequency is 4096 points/sec. Note that the forcing function repeats every one second.

Table 1 presents the test conditions and lubricant properties and Fig. 6 details the geometry of the SFD land.

**Table 1 Test conditions for dynamic load tests (CCO). Lubricated SFD (ISO VG 2)**

Inlet Pressure ( $P_s$ )*	31 kPa
Frequency Range	25, 30-120 Hz (sine sweep)
Lubricant temperature ( $T$ )	23-25 °C (73-77 °F)
Viscosity ( $\eta$ )	3.1 cP- 2.8 cP
Clearance ( $c$ )	122-125 $\mu\text{m}$ (4.8-4.9 mil)
Motion amplitude ( $ e $ )	20-60 $\mu\text{m}$ (0.8-2.4 mil)

\*: Gauge pressure.



**Figure 6 Detail view of test squeeze film damper geometry (open end)**

Figure 7 shows a schematic view of the equivalent mechanical system representation of the SFD.

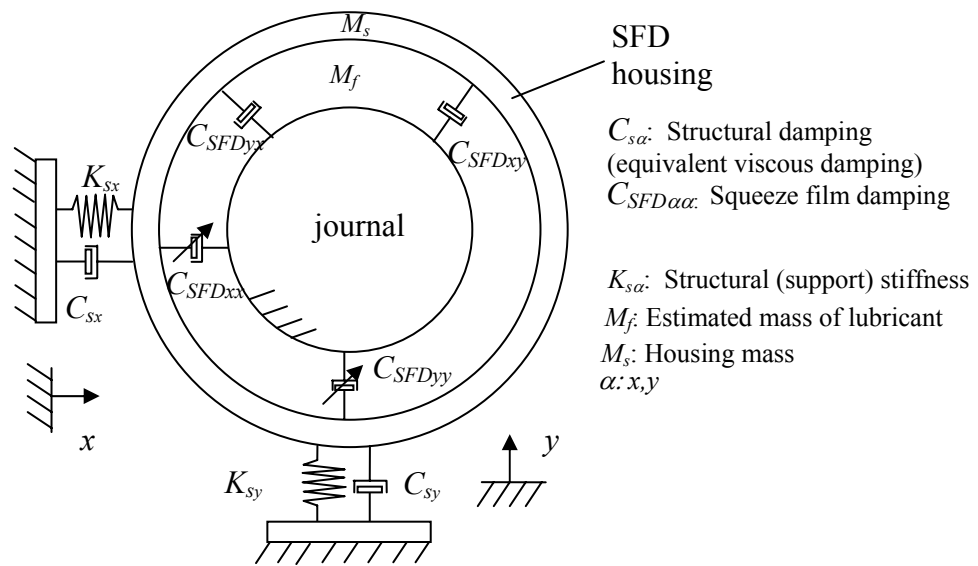


**Figure 7 Schematic view of the equivalent representation of the SFD with mechanical seal**

The equations of motion for the test bearing section are [4]

$$\begin{bmatrix} M & 0 \\ 0 & M \end{bmatrix} \begin{Bmatrix} \ddot{x} \\ \ddot{y} \end{Bmatrix} + \begin{Bmatrix} C_{sx} \dot{x} \\ C_{sy} \dot{y} \end{Bmatrix} + \begin{Bmatrix} K_{sx} x \\ K_{sy} y \end{Bmatrix} = \begin{Bmatrix} F_x \\ F_y \end{Bmatrix} - \begin{Bmatrix} F_x \\ F_y \end{Bmatrix}_{seal} - \begin{Bmatrix} F_x \\ F_y \end{Bmatrix}_{SFD} \quad (3)$$

Above  $M = M_s + M_f = 10.2 \text{ kg}$  ; where  $M_s$  is the mass of the vibrating structure and  $M_f$  is the mass of fluid enclosed in the plenum above the fluid film land section.  $(C_s)_{x,y}$  are the equivalent viscous damping coefficients that characterize the damping arising from the structural support. These coefficients, obtained from impact tests on the dry structure, equal 130 N.s/m, see Appendix A.

The SFD reaction forces are

$$\begin{Bmatrix} F_x \\ F_y \end{Bmatrix}_{SFD} = \begin{bmatrix} C_{SFD_{xx}(e)} & C_{SFD_{xy}(e)} \\ C_{SFD_{yx}(e)} & C_{SFD_{yy}(e)} \end{bmatrix} \begin{Bmatrix} \dot{x} \\ \dot{y} \end{Bmatrix} + \begin{bmatrix} M_{SFD_{xx}} & M_{SFD_{xy}} \\ M_{SFD_{yx}} & M_{SFD_{yy}} \end{bmatrix} \begin{Bmatrix} \ddot{x} \\ \ddot{y} \end{Bmatrix} \quad (4)$$

where  $e = f(x_{(t)}, y_{(t)})$  is the journal center instantaneous position and  $\{C_{SFD\alpha\beta}\}_{\alpha\beta=x,y}$   $\{M_{SFD\alpha\beta}\}_{\alpha\beta=x,y}$  are the squeeze film damping and inertia force coefficients, respectively. The mass coefficients can be approximated to a constant value for the range of test orbit amplitudes (i.e. up to 60 % of the damper clearance) [20].

The multiple frequency load excitations in Eq. (1) can be expressed in complex form as

$$F_x(t) = \sum_{k=1}^M (F_{xc} - iF_{xs})_k e^{i\omega_k t} = \sum_{k=0}^M (\bar{F}_x)_k e^{i\omega_k t} \quad (5)$$

$$F_y(t) = \sum_{k=1}^M (F_{yc} - iF_{ys})_k e^{i\omega_k t} = \sum_{k=0}^M (\bar{F}_y)_k e^{i\omega_k t}$$

and the ensuing bearing displacement (i.e.  $x$  and  $y$ ) as

$$\mathbf{Z}_{(\omega)} = \begin{Bmatrix} x \\ y \end{Bmatrix} = \sum_{k=0}^M \begin{Bmatrix} \bar{x}_k \\ \bar{y}_k \end{Bmatrix} e^{i\omega_k t} \quad (6)$$

where  $(\bar{x}, \bar{y})$ , and  $(\bar{F}_x, \bar{F}_y)$  are the discrete Fourier Transform (DFT) of the time varying displacements and forces, respectively.

Note that the damping coefficients are generalized functions of the journal instantaneous position. Thus, the damping force depends on the magnitude and direction of the velocity vector as well as on the instantaneous position of the journal center. Since the journal eccentricity is a periodic function, the damping coefficients can also be represented as a periodic function. Furthermore, the multiplication of the damping

coefficient and the velocity vector components (i.e. two periodic functions) can be expressed in the frequency domain as the summation of multiple frequency components,

$$\begin{aligned} F_{D_x}(e, \omega, \dot{x}) &= \alpha_{1x_k} \bar{x}_k \omega e^{\omega_k t} + \alpha_{2x_k} \bar{x}_k \omega e^{3\omega_k t} + \dots + \alpha_{nx_k} \bar{x}_k \omega e^{(2n-1)\omega_k t} \\ F_{D_y}(e, \omega, \dot{y}) &= \alpha_{1y_k} \bar{y}_k \omega e^{\omega_k t} + \alpha_{2y_k} \bar{y}_k \omega e^{3\omega_k t} + \dots + \alpha_{ny_k} \bar{y}_k \omega e^{(2n-1)\omega_k t} \end{aligned} \quad (7)$$

The damping force includes the frequency that coincides with the (force) excitation frequency (i.e. 1X component of the sine sweep) in order to dissipate energy. **Considering that the work input into the system is related to the main excitation frequency (i.e. 1X), the damping coefficients can be directly extracted from the imaginary part of the transfer function<sup>1</sup>.** Thus, for each individual frequency component the damping coefficient corresponds to the first frequency component of the dissipative force (i.e.  $\alpha_{1ij_k} = C_{SFD_{ij \ i,j:x,y}}$ ). Substituting Eq.(5) and Eq. (6) into the EOM Eq. (3) and **separating for each frequency component of the sine sweep excitation force yields**

$$\begin{aligned} \bar{F}_x &= H_{xx} \bar{x} + H_{xy} \bar{y} \\ \bar{F}_y &= H_{yy} \bar{y} + H_{yx} \bar{x} \end{aligned} \quad (8)$$

where the impedance functions  $H$  are defined as

$$H_{ij} = K_{Si} - M_{s-ij} \omega^2 + i \omega C_{s-ij} ; \quad i, j = x, y \quad (9)$$

with

$$\begin{aligned} M_{s-ii} &= M_{SFD_i} + M \\ C_{s-ii} &= C_{SFD_i} + C_{si} ; \quad C_{s-ij} = C_{SFD_j} ; \quad i, j = x, y \end{aligned} \quad (10)$$

The system damping coefficients ( $C_{s-ij}$ ) are a function of frequency since the displacement amplitude also varies with frequency. Thus, the damping coefficients in Eq. (10) can not be estimated with a single parameter as in the case of circular journal motions about a centered position, for example.

The impedance functions  $H_{ij}$  are identified from three different force excitation vectors using a combination of the multiple frequency sine sweep excitation loads presented in Eq. (1). For all test cases, the identification range is limited to frequencies from 40 to 80 Hz. This limitation is due to the fact that when using sine sweep excitations

---

<sup>1</sup> **Note from Editor:** The paragraph is incomprehensible as per its physical or mathematical rationale

it is not possible to discern the contribution of the components of higher order (2X, 3X) to the (1X) input excitation frequency. This range is appropriate to characterize intershaft dampers since it includes the natural frequency of the system (~50 Hz) and covers from 2X to 3X of the fixed frequency (25 Hz) representing the low speed shaft.

The identified damping coefficients are compared to well-known formulas for open-ends SFDs (Ref. [18]) for two cases: circular centered orbits (CCOs) and small amplitude displacements about an off-centered position (ORMs). Figure 8 depicts the predictions versus journal eccentricity and the corresponding equations valid for uncavitated films. Since the multiple frequency excitations exert a combination of radial and tangential journal motion paths, the damping coefficients are expected to be within the region enclosed between the limiting cases. The description of the experimental results and identified force coefficients follow.

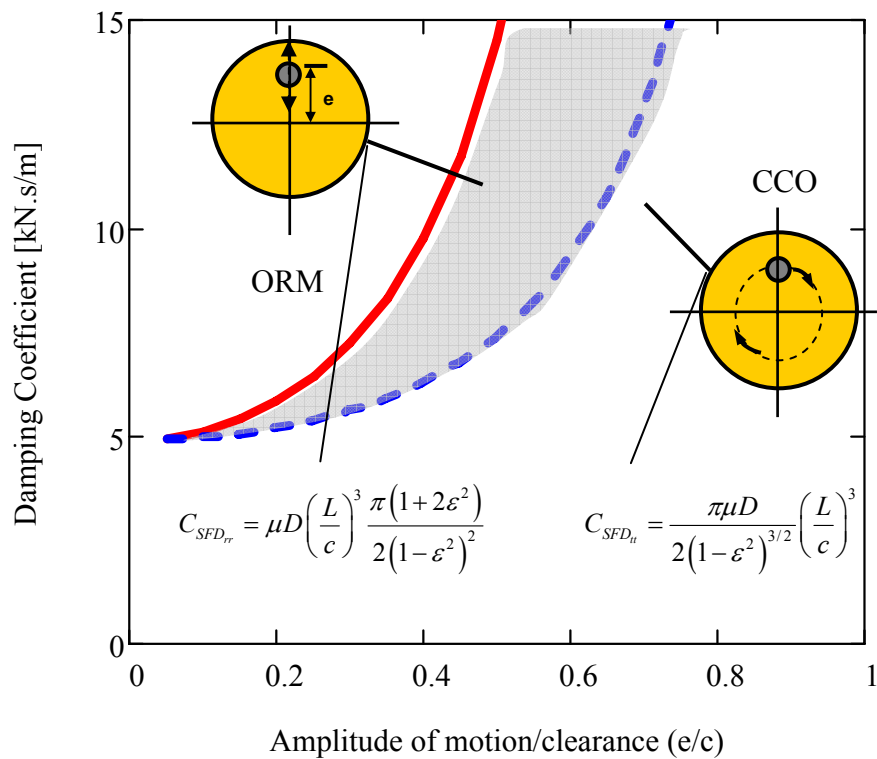


**Figure 8 Damping coefficient versus journal eccentricity for circular centered orbits and radial displacements about an off-centered position [18]**

## V Identified SFD Force Coefficients and Comparisons to Predictions

### Multiple Sine Sweep Excitations with Fixed Load Amplitude ( $F_1$ & $F_2$ )

For the first tests, the four impedance functions ( $H_{xx}$ ,  $H_{xy}$ ,  $H_{yy}$ ,  $H_{yx}$ ) are identified assuming that the cross-coupled coefficients are non zero (i.e. an oil cavitated damper). To identify the full set of impedance functions it is necessary to excite the system with two independent force excitation vectors. Considering that a damping coefficient is a function of the journal position, each excitation vector needs to induce similar journal motion amplitudes such that the direct impedance functions are similar for both excitations. A pair of force excitation vectors that meet these conditions is

$$\mathbf{F}_1 = \begin{pmatrix} F_{x_1} \\ F_{y_1} \end{pmatrix} = \begin{pmatrix} F_s(t) \\ F_s(t) \end{pmatrix}, \quad \mathbf{F}_2 = \begin{pmatrix} F_{x_2} \\ F_{y_2} \end{pmatrix} = \begin{pmatrix} F_s(t) \\ -F_s(t) \end{pmatrix} \quad (11)$$

with  $F_s(t)$  defined in Eq. (1). This pair of excitation vectors renders multiple frequency motions enclosed within elliptical envelope curves with the mayor axes oriented  $\theta=45^\circ$  and  $\theta=135^\circ$  from the  $X$  direction. In an intershaft system, this condition simulates the case where the motion response vector for each shaft is either in or out of phase with each other.

Force excitations  $\mathbf{F}_1$  and  $\mathbf{F}_2$  induce bearing motions and the impedance coefficients  $H$  are obtained from

$$\begin{bmatrix} H_{xx} & H_{xy} \\ H_{yx} & H_{yy} \end{bmatrix} = \begin{bmatrix} \bar{F}_{x_1} & \bar{F}_{x_2} \\ \bar{F}_{y_1} & \bar{F}_{y_2} \end{bmatrix} \begin{bmatrix} \bar{x}_1 & \bar{x}_2 \\ \bar{y}_1 & \bar{y}_2 \end{bmatrix}^{-1} \quad (12)$$

where  $(\bar{x}_i, \bar{y}_i)_{i=1,2}^T$  are the bearing displacement response due to the corresponding excitation load vector. The system impedance functions are identified and averaged from 30 sets of excitations built with  $\mathbf{F}_1$  and  $\mathbf{F}_2$ . This procedure is repeated three times to yield a single average set of impedance functions. The stiffness and added mass coefficients are identified from the real part of the impedance functions, Eq. (9), using a quadratic curve fit in terms of the response frequency,

$$K_{S_i} - M_{S-ij} \omega^2 = \text{Re}(H_{ij}) \quad (13)$$

The system damping coefficients are extracted from the imaginary part of the impedance functions,

$$C_{s-ij} = \frac{\text{Im}(H_{ij})}{\omega} = C_{SFD-ij} + C_{si} \quad (14)$$

Figures 9 and 10 depict the journal displacement path induced by the excitation vectors  $\mathbf{F}_1$  and  $\mathbf{F}_2$ , respectively. Notice that the motion paths over the sample period are overlapped and can not be clearly distinguished. The motion path is predominantly in the radial direction along the axes given by the equations  $x=y$  and  $x=-y$  ( $\theta=45^\circ$ ,  $\theta=135^\circ$ ). However, the multiple frequency motions are not purely radial. Figure 11 shows a representative time trace of the excitation loads and ensuing motions in both directions when exciting the system with  $\mathbf{F}_1$ . Figure 12 depicts the FFT of the loads and displacements shown in Fig. 11. The frequency spectra include a fixed excitation frequency (25 Hz) and sine sweep excitations (30 Hz- 120 Hz).

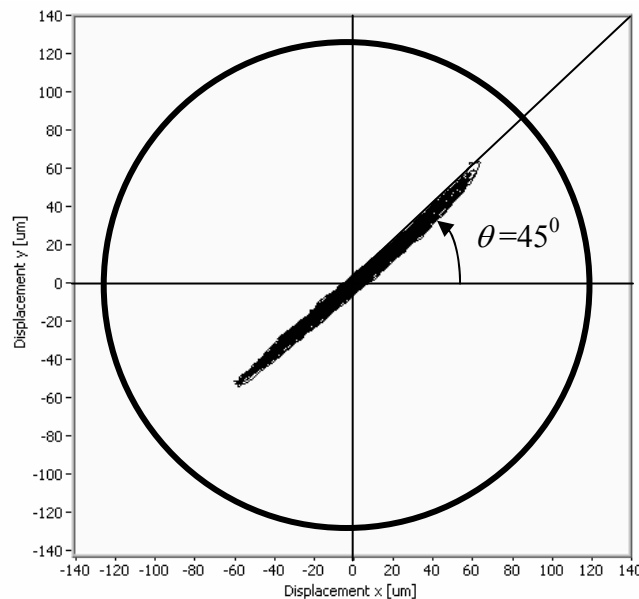


**Figure 9 Bearing displacements for three amplitude load magnitudes, force excitation vector  $F_1$ . Multiple frequency excitation (constant 25 Hz + chirp 30-120Hz). Clearance circle noted.**

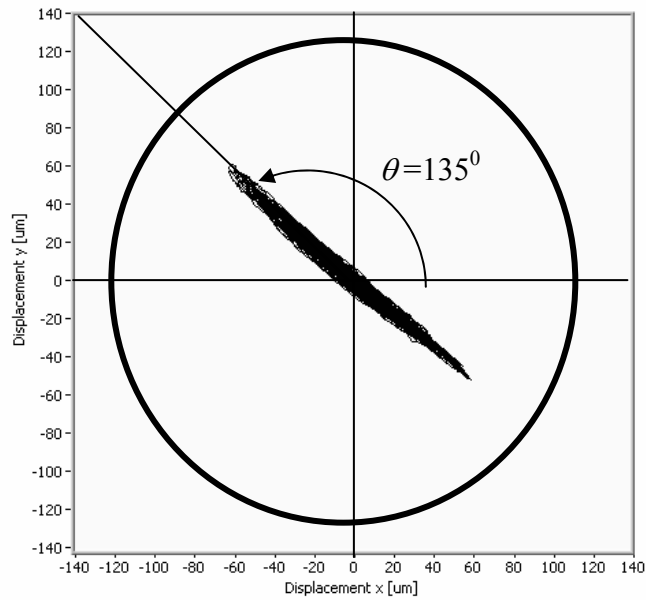


**Figure 10 Bearing displacements for three amplitude load magnitudes, force excitation vector  $F_2$ . Multiple frequency excitation (constant 25 Hz + chirp 30-120Hz). Clearance circle noted)**

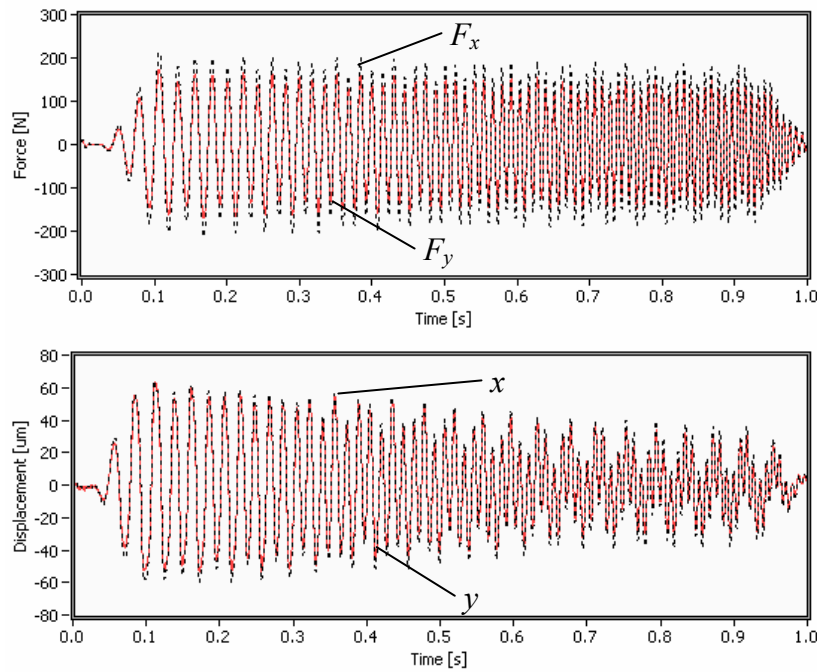


**Figure 11 X, Y Forces and ensuing X, Y displacements versus time. Excitation vector  $F_1$ . Multiple-frequency excitation (constant 25Hz + sine sweep 30-120Hz). (Maximum motion amplitude  $\sim 60 \mu\text{m}$ )**

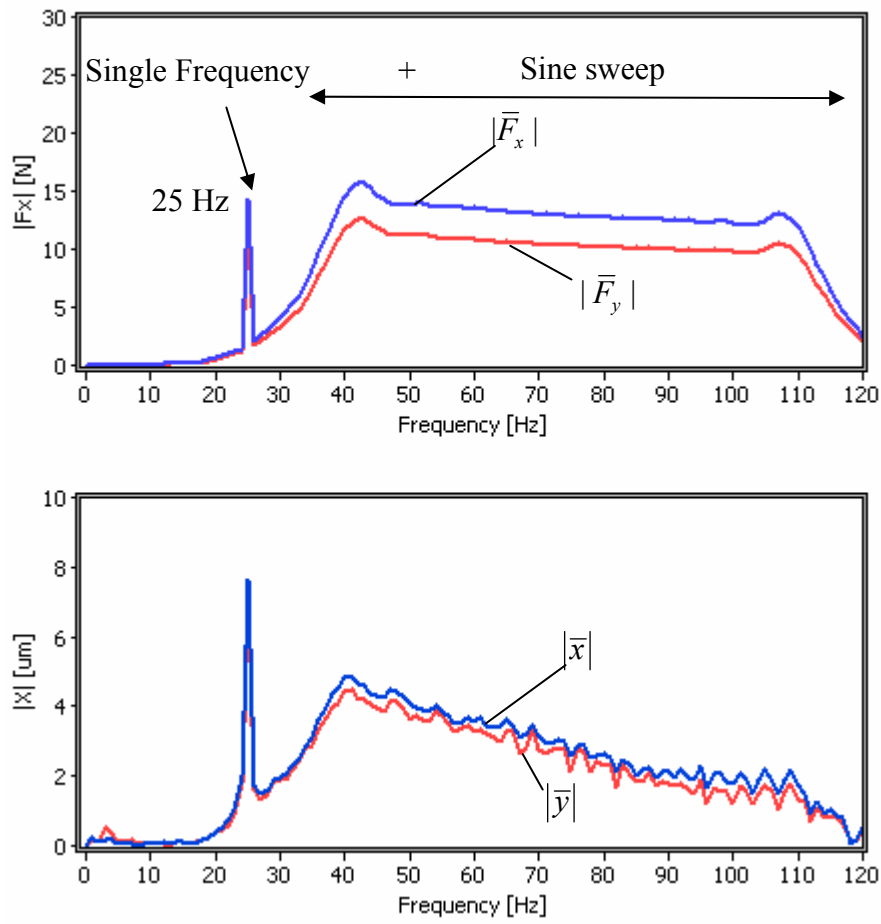


**Figure 12** FFT of input forces and ensuing displacements  $X$ ,  $Y$  due to excitation vector  $F_1$

Figure 13 depicts the real part of the direct impedance functions and the corresponding curve fit of the dynamic stiffness ( $K_{si} - M_{s-ii} \omega^2$ ;  $i=x,y$ ). Table 2 presents the identified mass coefficients and the extracted added mass coefficient associated to the squeeze film only. The table also shows the predicted added mass coefficient using the model in Ref. [9], which takes into account the effects of the inlet and discharge grooves on the dynamic forced response of the damper. The cross-coupled coefficients are rather small as expected for SFD operation in the absence of oil cavitation. Appendix B presents the cross-coupled impedance functions and the identified cross-coupled coefficients.

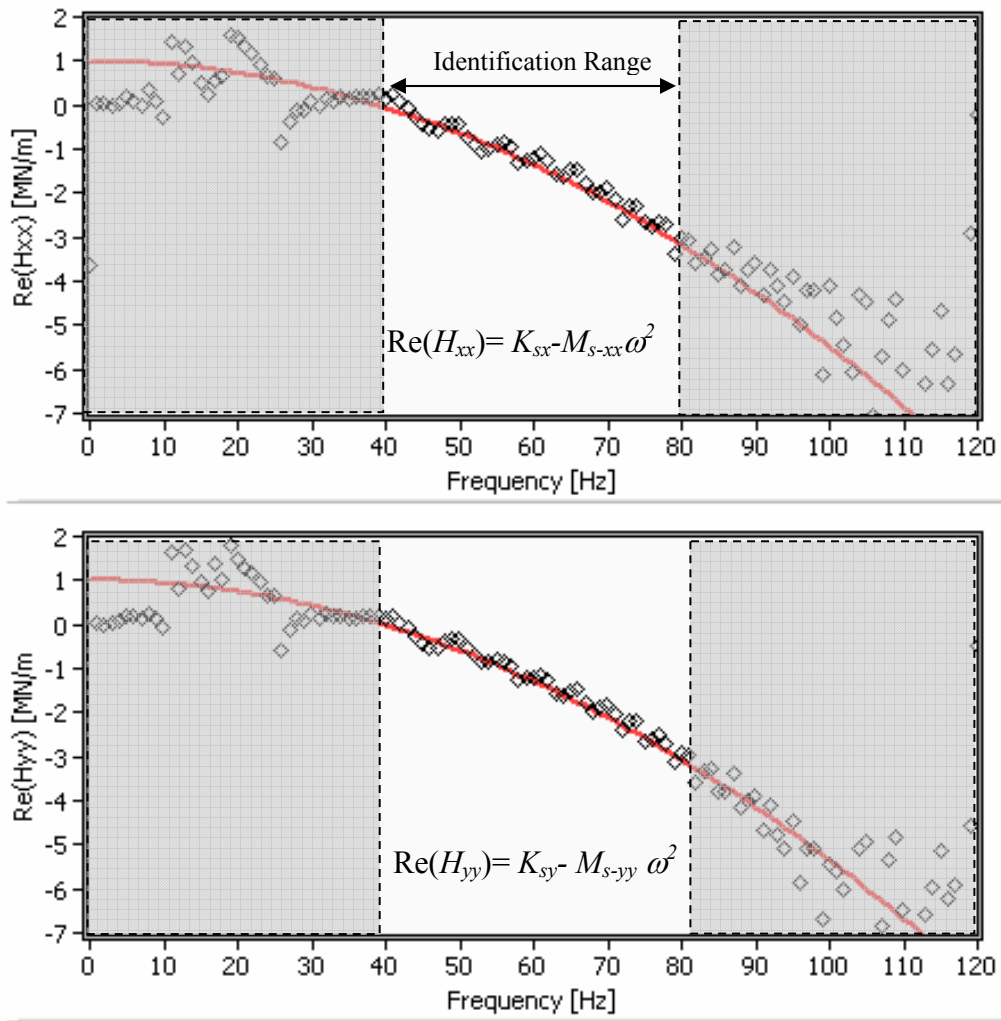


**Figure 13 Real part of direct impedances versus frequency. Multiple frequency excitation (constant 25Hz + sine sweep 30-120Hz). ( $K_{sx}= 860$  kN/m,  $K_{sy}= 890$  kN/m). Excitation vectors  $F_1$  &  $F_2$**

**Table 2 SFD inertia coefficients identified from non-circular centered orbit tests (frequency range 40-80 Hz) ( $K_{sx}= 860$  kN/m,  $K_{sy}= 890$  kN/m)**

Parameter	<i>xx</i>	<i>yy</i>
Identified Mass, ( $M_s$ )	<b>16.3 kg</b>	<b>16.1kg</b>
Squeeze film inertia ( $M_{SFD}$ )	<b>6.1 kg</b>	<b>5.9 kg</b>
$r^2$ (goodness of curve fit)	0.97	0.98
System Mass, ( $M_s$ ) [kg]	9.6	
Fluid Mass, ( $M_f$ ) [kg]	0.62	
Added mass coefficient (Predictions from Ref.[9])	<b>6.6 kg</b>	

Figure 14 shows the imaginary part of the direct impedance functions divided by the excitation frequency ( $\omega$ ). The damping coefficients ( $C_{SFDxx}$  and  $C_{SFDyy}$ ) decay throughout the frequency identification range with a similar trend to that shown in the frequency spectra of the journal displacements shown in Fig. 12. This is, as expected, a clear indication of the dependency of the squeeze film damping coefficients on the amplitude of journal motions.

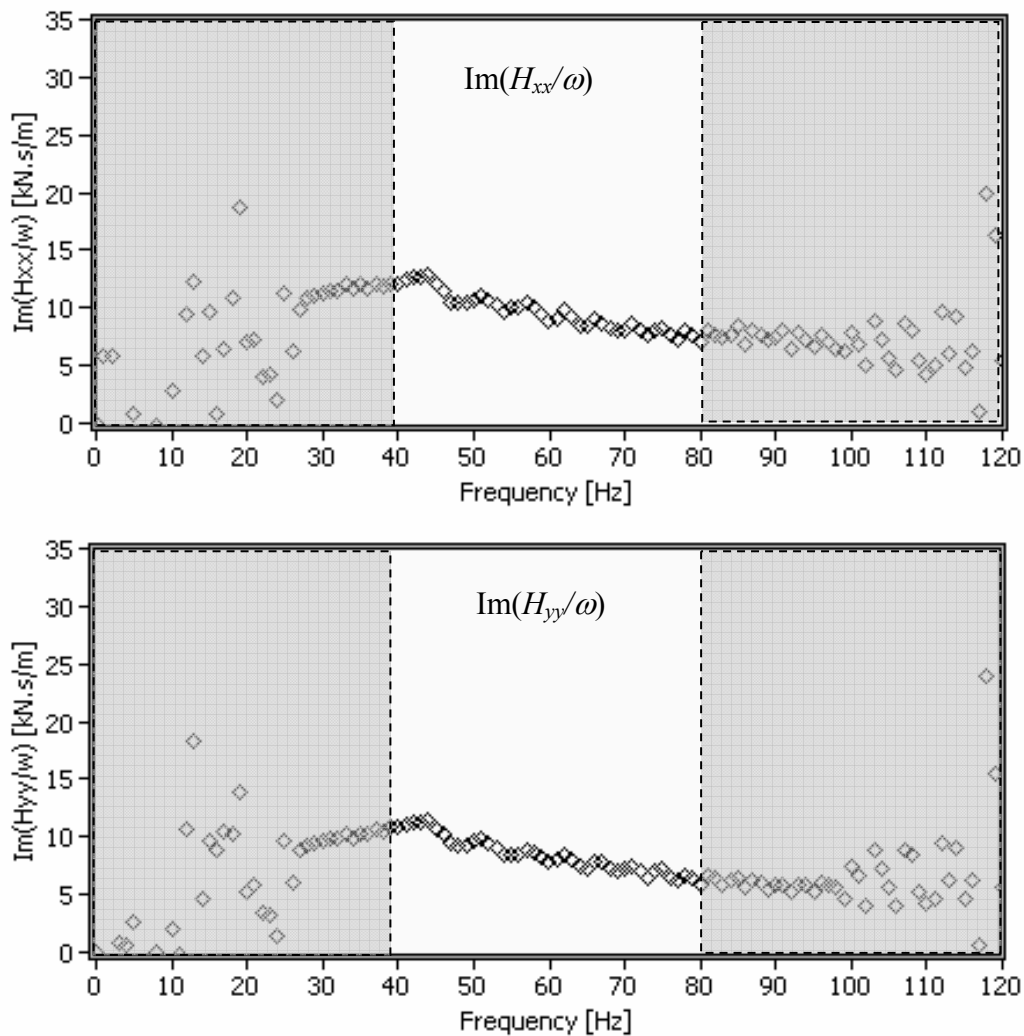


**Figure 14 Imaginary part of direct impedances  $\times (1/\omega)$  versus excitation frequency. Multiple frequency excitation (constant 25Hz + sine sweep 30-120Hz). Excitation vectors  $F_1$  &  $F_2$**

Figure 15 presents the identified damping coefficients  $C_{SFDxx}$  and  $C_{SFDyy}$  versus amplitude of journal motion. The figure also includes the damping coefficients for the

two limiting cases: circular centered orbits (CCOs) and radial motions about an off-centered journal position (ORMs).

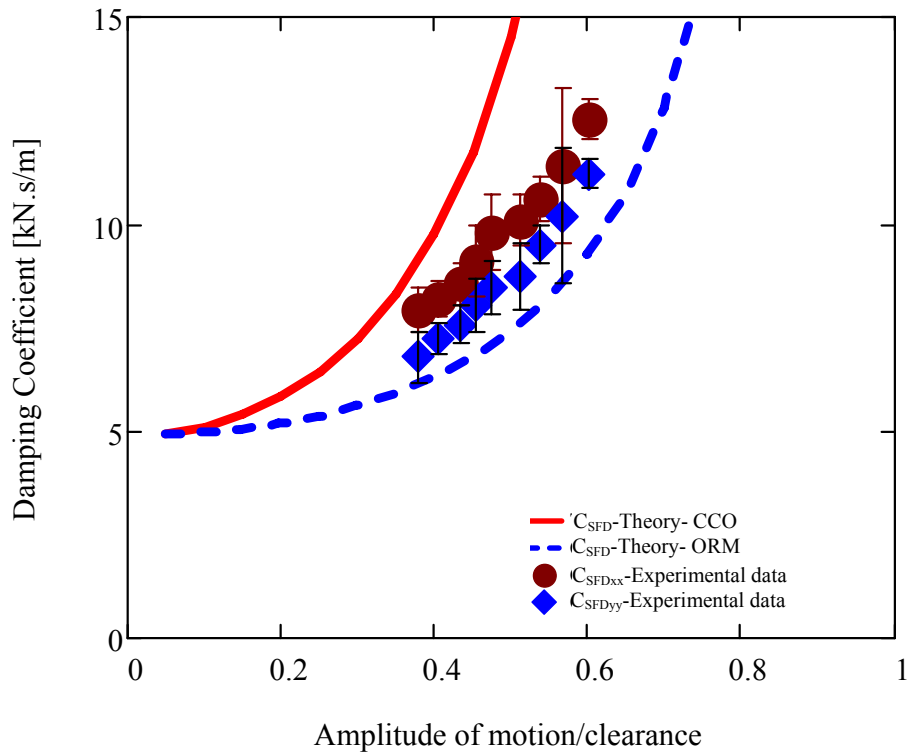


**Figure 15 Direct squeeze film damping coefficients identified from fixed load amplitude, multiple frequency load excitations. (25Hz + sine sweep 30-120Hz). Excitation vectors  $F_1$  &  $F_2$ ). Predictions for circular centered orbits (CCO) and radial motion about an off-centered journal position**

### Sine Sweep Excitations with Varying Load Amplitude ( $F_1$ & $F_2$ )

In the following, the amplitude of the excitation load vector increases with excitation frequency such as to induce a constant amplitude journal motion throughout the identification frequency range. The varying amplitude of load, see Eq. (1), increases linearly with time as shown in Fig. 16 through 18. Figure 19 depicts the frequency spectrum representative of each set of tests (~15, 30, 50  $\mu\text{m}$ ).

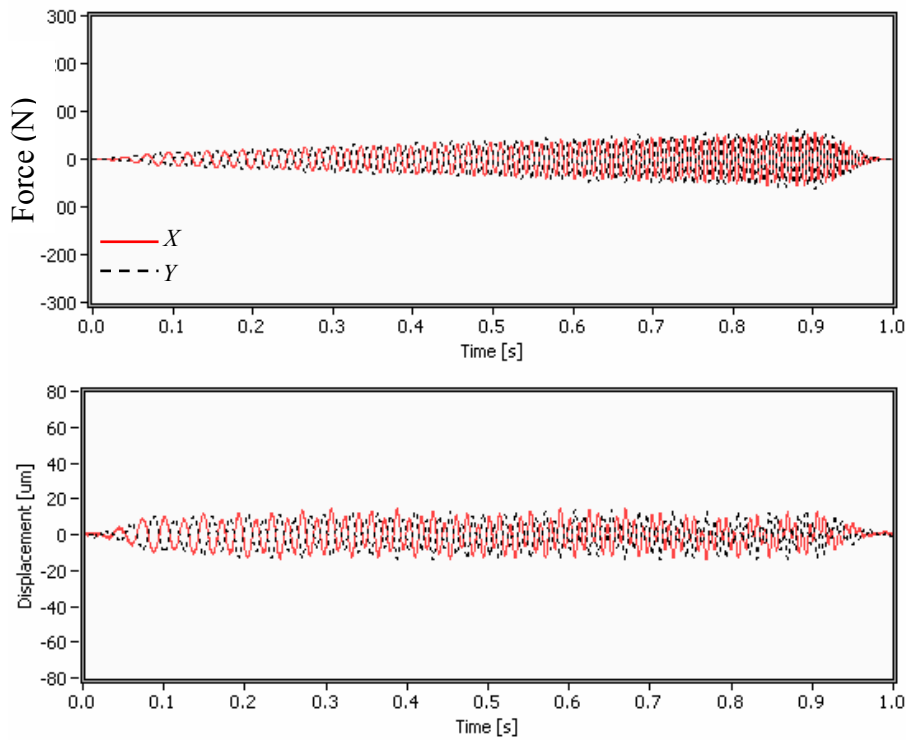


**Figure 16** Excitation forces  $F_X$ ,  $F_Y$  and ensuing  $X$ ,  $Y$  bearing displacements versus time (Set maximum journal amplitude  $\sim 15 \mu\text{m}$ )

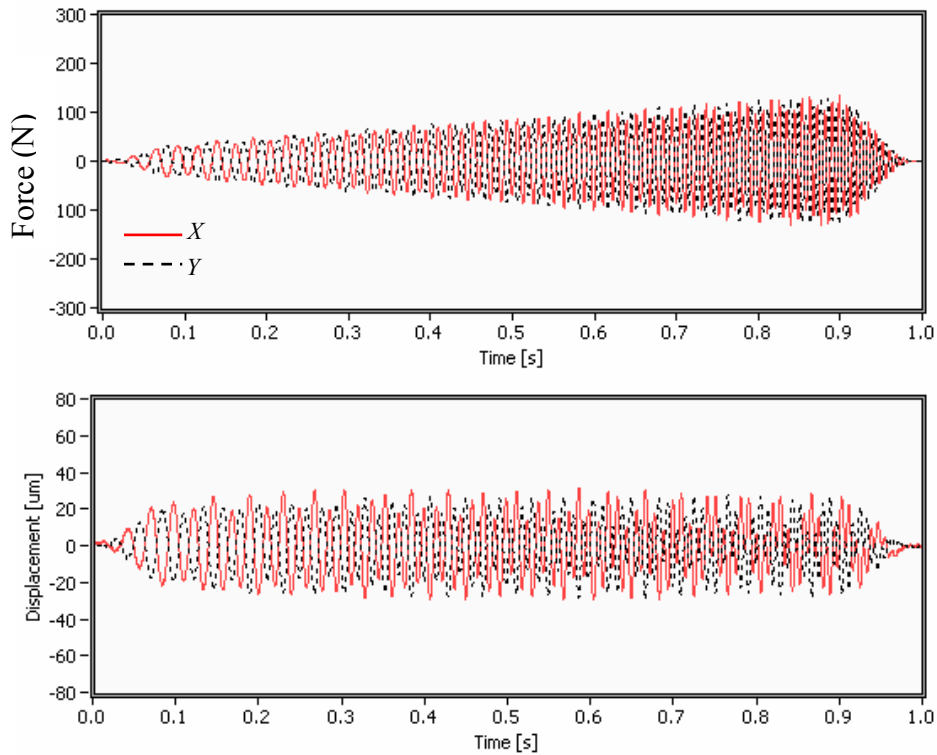


**Figure 17** Excitation forces  $F_X$ ,  $F_Y$  and ensuing  $X$ ,  $Y$  bearing displacements versus time (Set maximum journal amplitude  $\sim 30 \mu\text{m}$ )

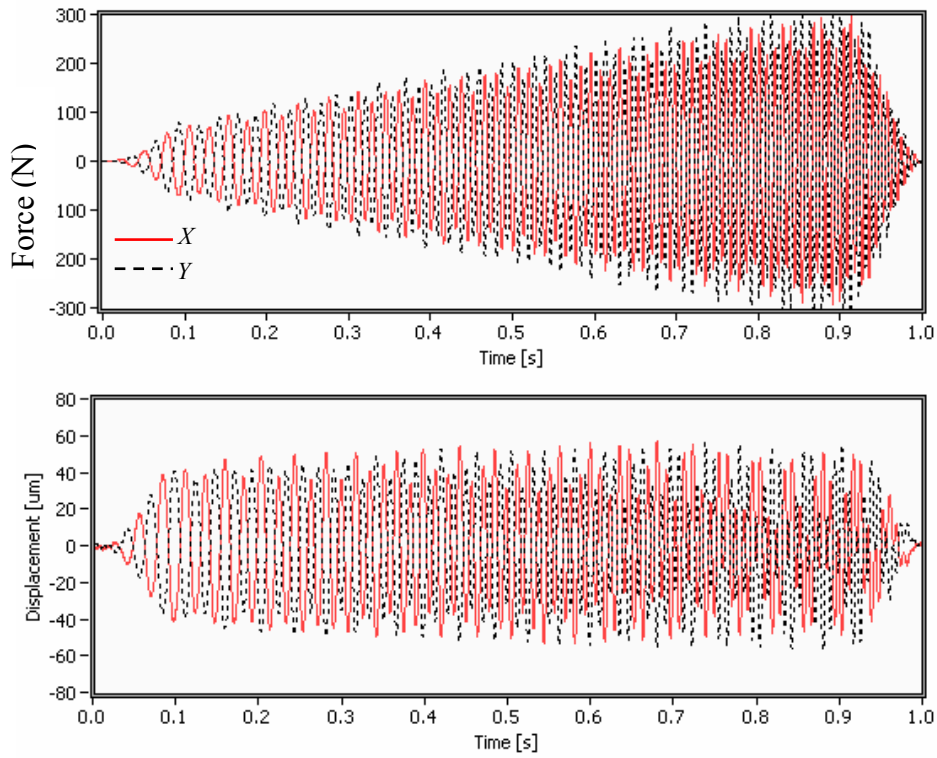


**Figure 18** Excitation forces  $F_x$ ,  $F_y$  and ensuing  $X$ ,  $Y$  bearing displacements versus time (Set maximum journal amplitude  $\sim 50 \mu\text{m}$ ).

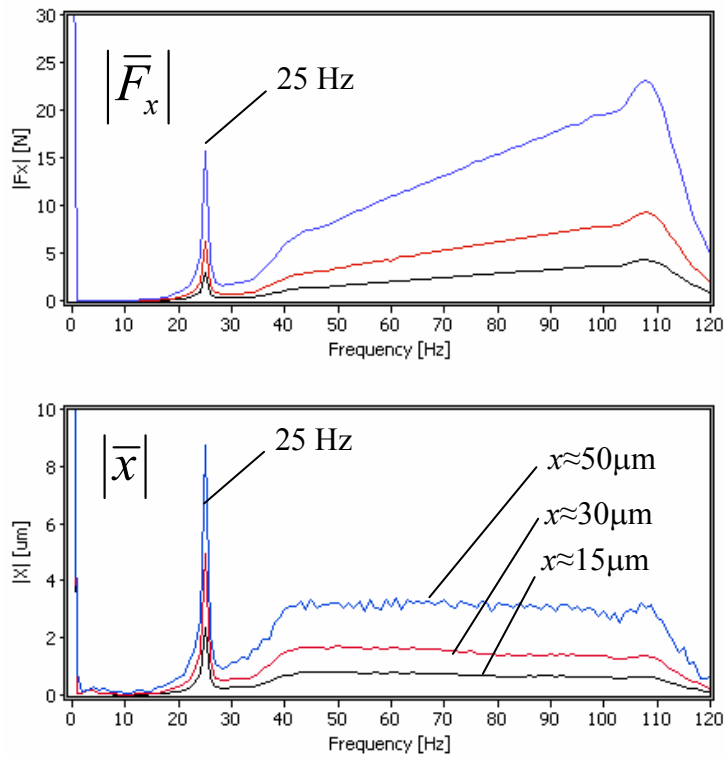


**Figure 19** Frequency spectra of  $X$ -force and ensuing  $X$ -displacement. Time data shown in Figures 16-18

Figure 20 shows the imaginary part of the direct impedances versus frequencies for the tests with sine sweep excitation loads of increasing amplitude. The results show that the imaginary part of the transfer function ( $F_x/x$ ) can be approximated with a line fit. Thus, the direct damping coefficients are readily identified as the slope of the curve fit, i.e.

$$\text{Im}(H_{ii}) - C_{si} = \omega C_{SFDi} \quad ; \quad i = x, y \quad (15)$$

This indicates that the damping can be represented with a single coefficient as long as the amplitude of journal motion is constant throughout the identification frequency range. Table 3 presents the identified mass coefficients and the squeeze film added mass coefficients ( $M_{SFDxx}$ ,  $M_{SFDyy}$ ). Notice that the identified added mass coefficients are similar to those presented in Table 2, and also correlate well with a prediction of 6.6 kg, see Table 2.

**Table 3 SFD inertia coefficients identified from non-circular centered orbit tests (frequency range 40-80 Hz). Varying load amplitude**

Max. displ. Amplitude ( $ X ,  Y $ )	20 $\mu\text{m}$	40 $\mu\text{m}$	60 $\mu\text{m}$	$R^2$
$M_{xx}$	16.1 kg	16.1 kg	16.2 kg	0.99
$M_{SFDxx}$	<b>5.9 kg</b>			
$M_{yy}$	15.8 kg	15.9 kg	16.1 kg	0.99
$M_{SFDyy}$	<b>5.8 kg</b>			

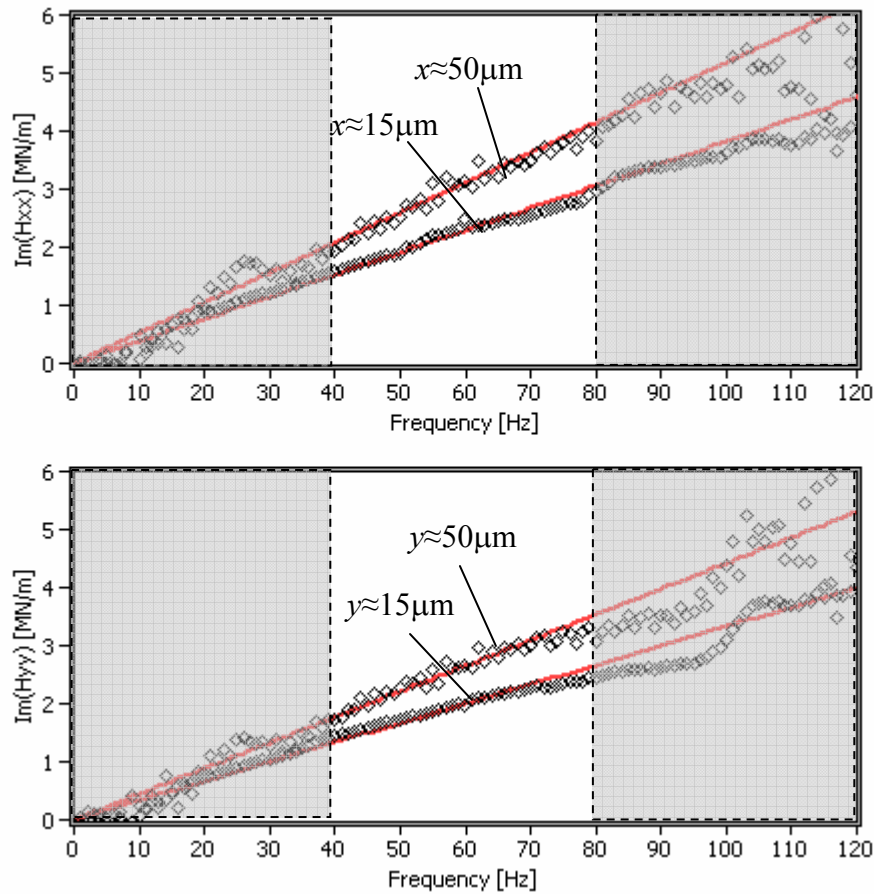


**Figure 20** Imaginary part of impedance functions,  $\text{Im}(F_x/X)$  &  $\text{Im}(F_y/Y)$ . Non-circular orbits, multiple frequency load excitations. Maximum displacement amplitudes: 15  $\mu\text{m}$  and 50  $\mu\text{m}$ .

Table 4 presents the damping coefficients identified from the sine sweep load excitations forcing constant amplitude journal motions. The uncertainty associated to the estimated squeeze film damping coefficients (i.e. slope of curve fit) is presented for a 95 % confidence interval, as in Ref. [21].

**Table 4** Damping coefficients estimated from fixed (set) SFD amplitudes (varying load amplitude) tests

Constant displacement amplitude	Amplitude	15 $\mu\text{m}$	30 $\mu\text{m}$	50 $\mu\text{m}$
	$C_{SFDxx}$ [N.s/m]		6,100( $\pm$ 300)	6,400( $\pm$ 400)
	$C_{SFDyy}$ [N.s/m]	5,300( $\pm$ 600)	5,500( $\pm$ 500)	7,000( $\pm$ 700)

Figure 21 depicts the damping coefficients identified from the varying excitation force amplitude. The figure also includes the predicted damping coefficients for CCOs

and ORMs. The identified damping coefficients for the largest test journal amplitude are slightly smaller (~20 %) than those identified in the previous section using constant load amplitude, multiple frequency excitations. The small discrepancy is expected since for both experiments the journal follows different motion paths. Furthermore, the motions exerted by the constant load excitation include larger variations of the journal motion amplitude (i.e. motions with a larger radial component) when compared to the experiments with increasing load amplitudes and relatively constant journal motion amplitudes.

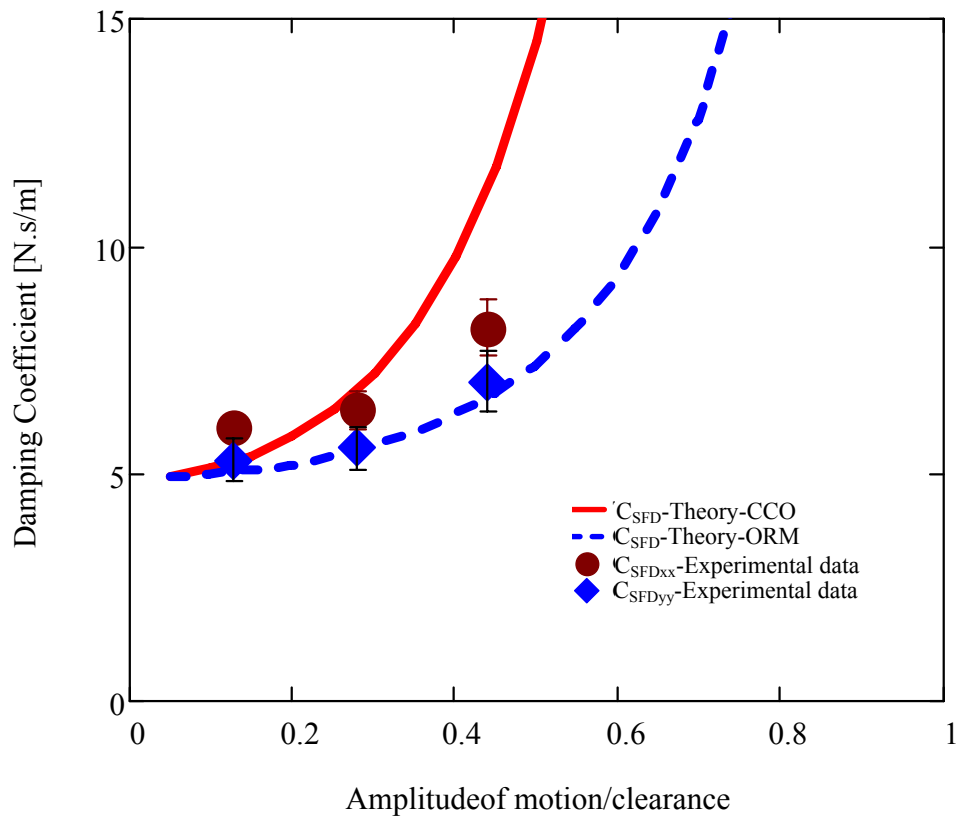


**Figure 21 Direct squeeze film damping coefficients identified from varying load amplitude, multiple frequency load excitations. (25Hz + sine sweep 30-120Hz). Predictions for circular centered orbits (CCO) and radial motion about an off-centered journal position**

### Sine Sweep Excitations with Rotating Load Vector $F_3$

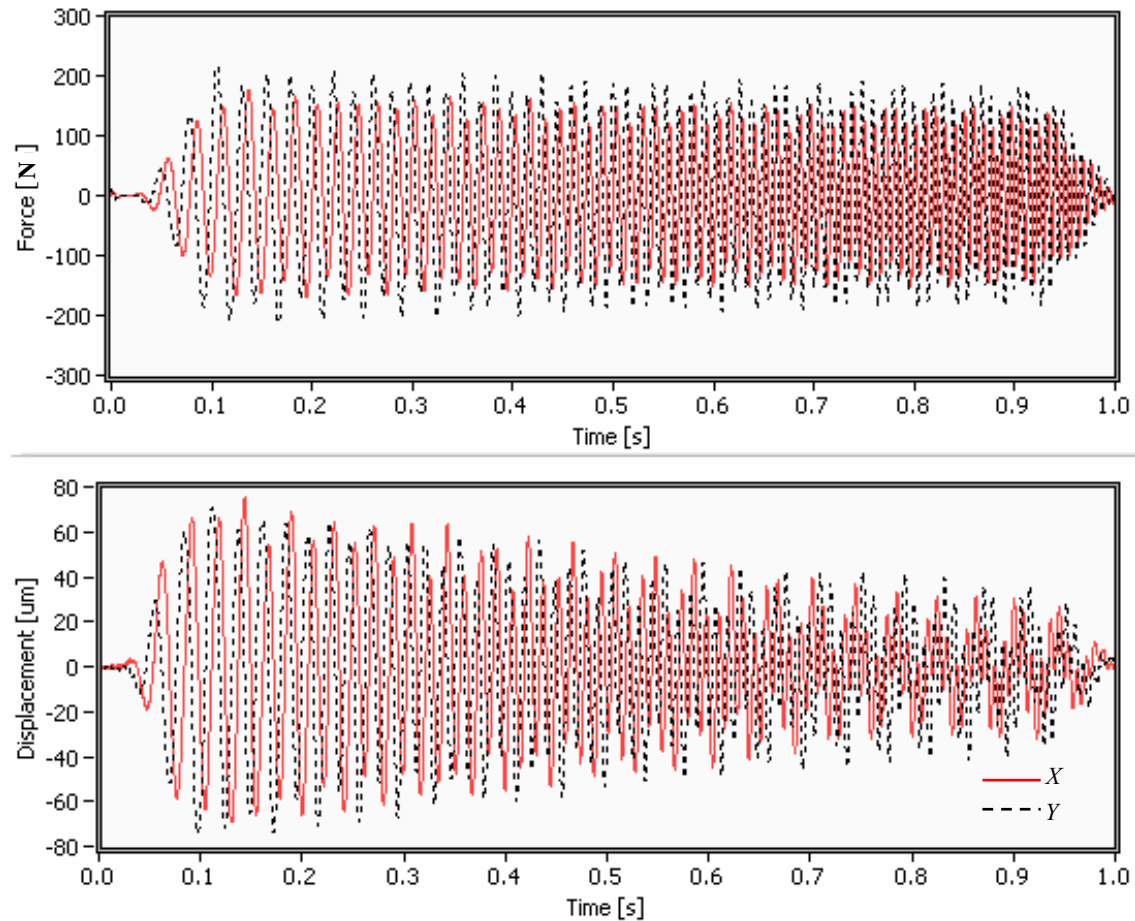
For this case, non-circular bearing motions are induced by the multiple frequency force vector:

$$\mathbf{F}_3 = \begin{pmatrix} F_x \\ F_y \end{pmatrix} = \begin{pmatrix} F_s(t) \\ F_c(t) \end{pmatrix} \quad (16)$$

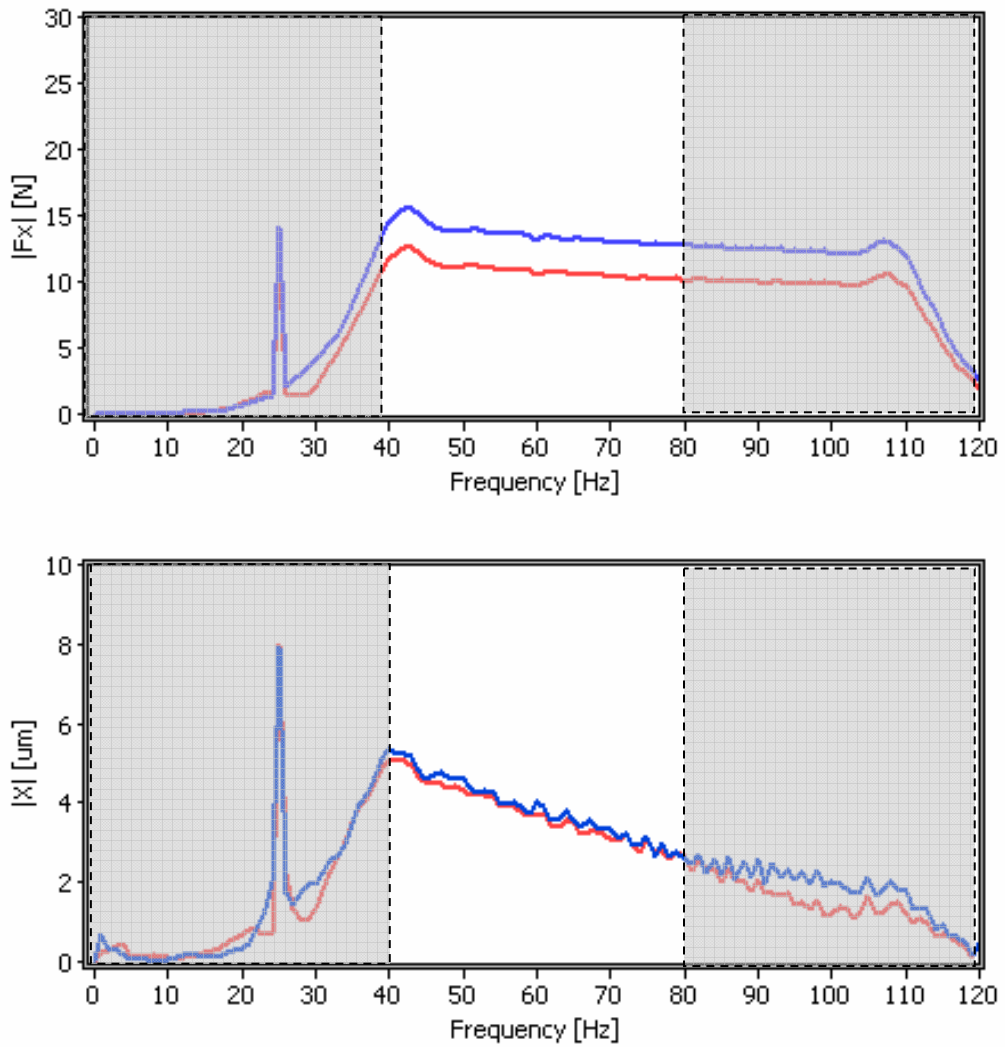
$$\begin{aligned} F_s(t) &= A \sin(2\pi f_0 t) + B \sin(2\pi f_1(t)t); \\ F_c(t) &= A \cos(2\pi f_0 t) + B \cos(2\pi f_1(t)t); \end{aligned} \quad (1)$$

That is, the  $y$ -force lags by  $90^\circ$  the  $x$ -force (excitation vector  $\mathbf{F}_3$ ). The force vector describes circular loads, as with a rotating imbalance, for example.

Figure 22 shows the multiple frequency excitation load and ensuing displacements versus time. Figure 23 depicts the frequency spectra of the excitation force and ensuing displacements. Notice that the excitation force amplitude is nearly constant within the frequency range of 40-80 Hz, while the displacement amplitude steadily decays with frequency.

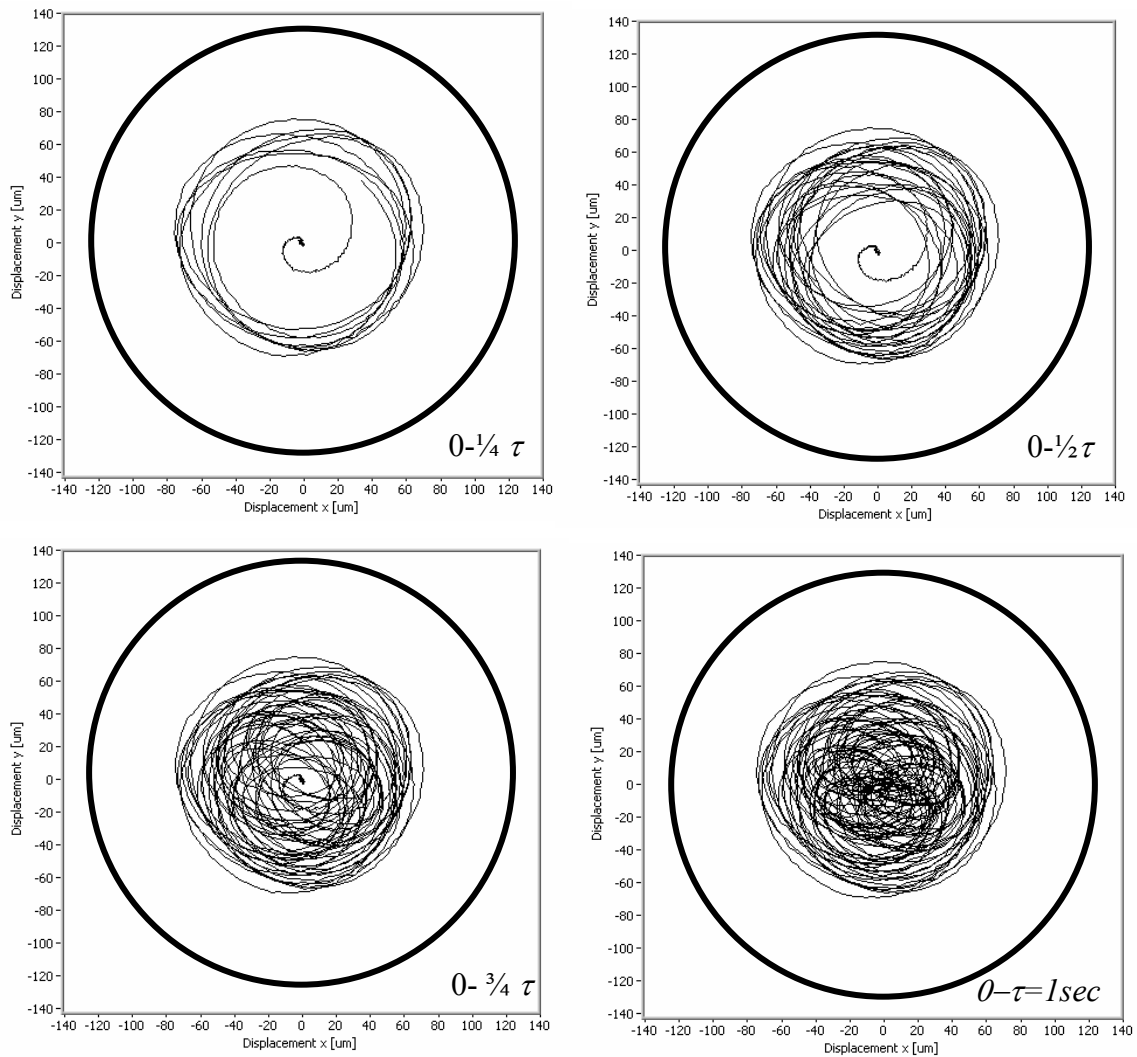


**Figure 22 Excitation forces  $F_x$ ,  $F_y$  and ensuing  $X$ ,  $Y$  bearing displacements versus time. Excitation vector  $\mathbf{F}_3$ : rotating load, sine sweep frequency**



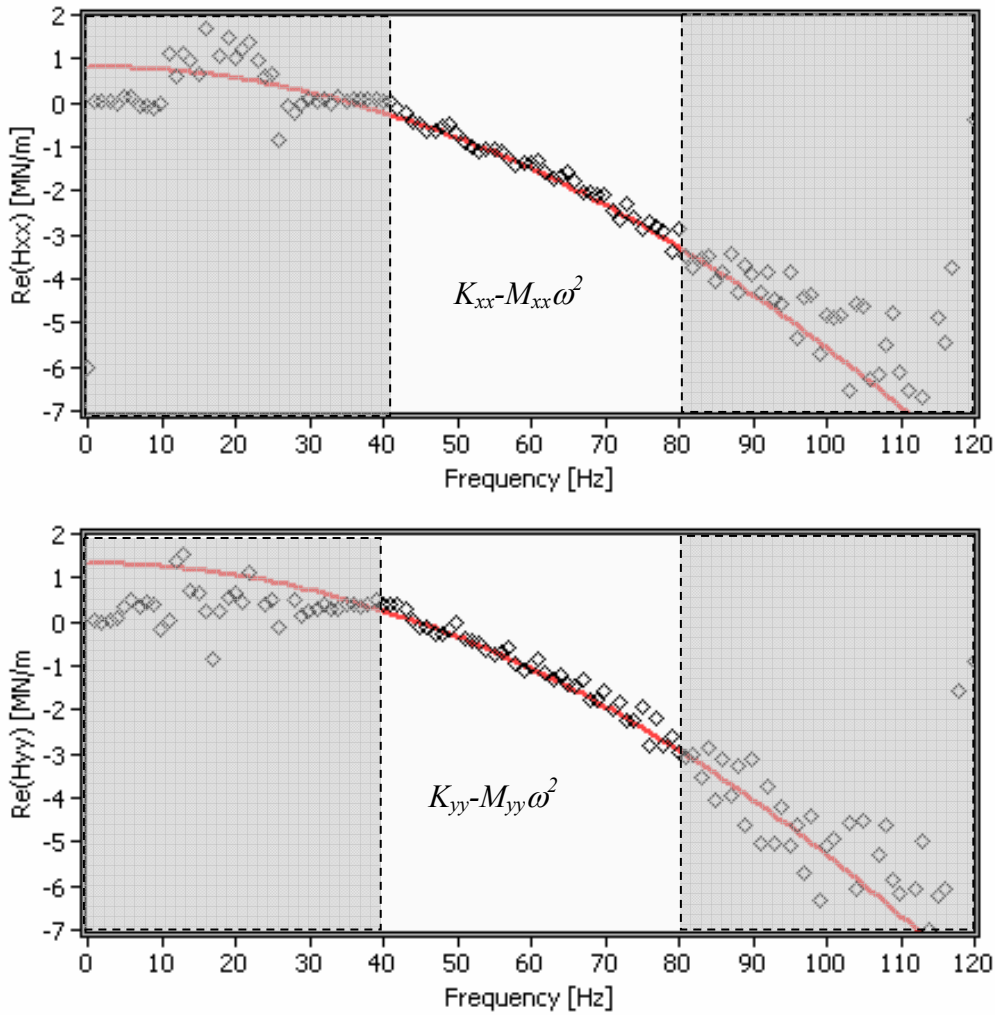
**Figure 23 Frequency spectra of X&Y forces and ensuing X&Y displacements. Time data shown in Figure 22. rotating load vector  $F_3$**

Figure 24 shows a sequence of the journal center path for a full 1 second when exciting the system with  $F_3$ . The maximum amplitude is  $70 \mu\text{m}$ , around 60 % of the damper clearance.



**Figure 24 Recorded bearing orbits due to rotating load vector  $F_3$ . Motions shown for time intervals  $0-1/4\tau$ ,  $0-1/2\tau$ ,  $0-3/4\tau$ ,  $0-1\tau$ . Multi-frequency excitation (constant 25 Hz + sine sweep 30-120Hz). Clearance circle noted.**

Figure 25 shows the real part of the impedance function identified from the tests and the curve fit of the dynamic stiffness. Table 5 presents the identified system mass coefficients and the squeeze film added mass coefficients. The identified values are similar to those obtained in the previous cases with different force excitations.



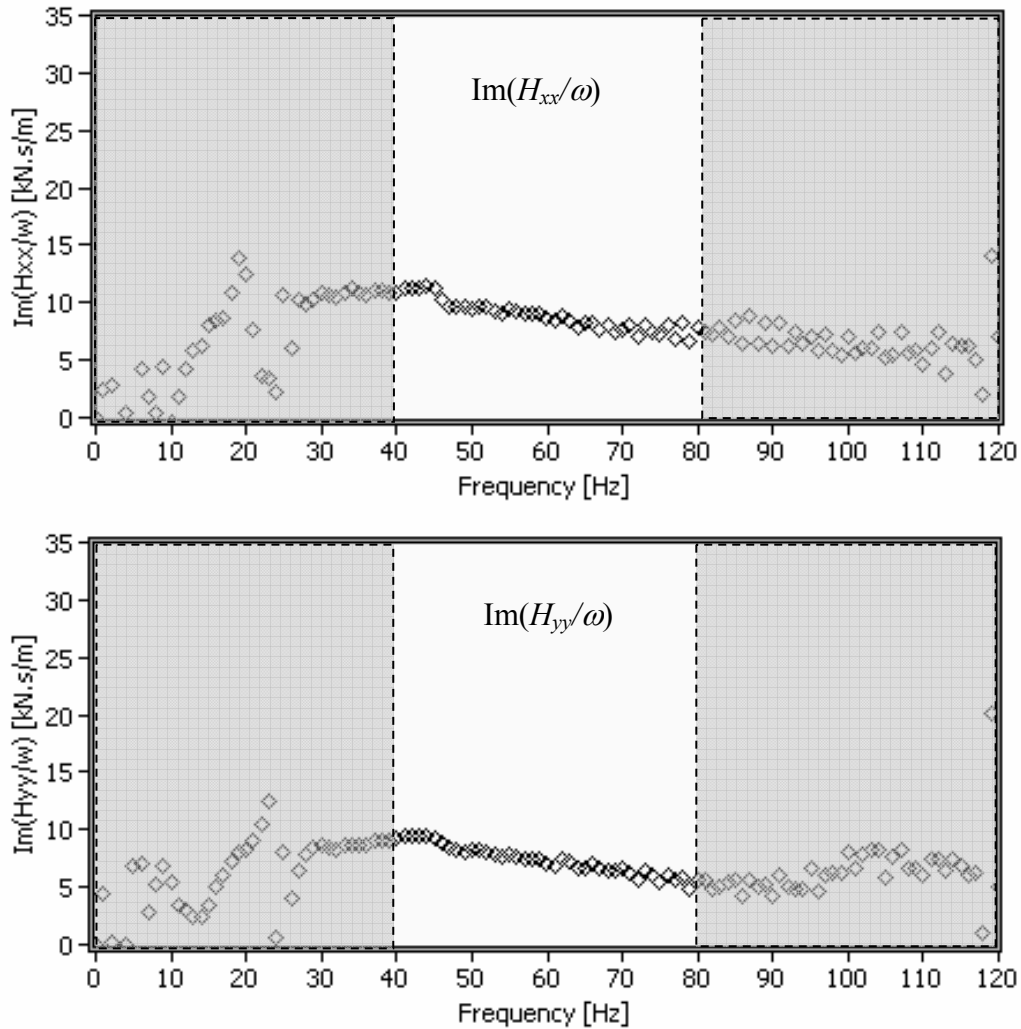
**Figure 25 Real part of direct impedances versus frequency. Constant amplitude rotating load with multiple frequency sine sweep excitation ( $K_{sx}= 860$  kN/m,  $K_{sy}= 890$  kN/m)**

**Table 5 SFD inertia coefficients identified from rotating load of constant amplitude rotating load with multiple frequency sine sweep excitation (frequency range 40-80 Hz)**

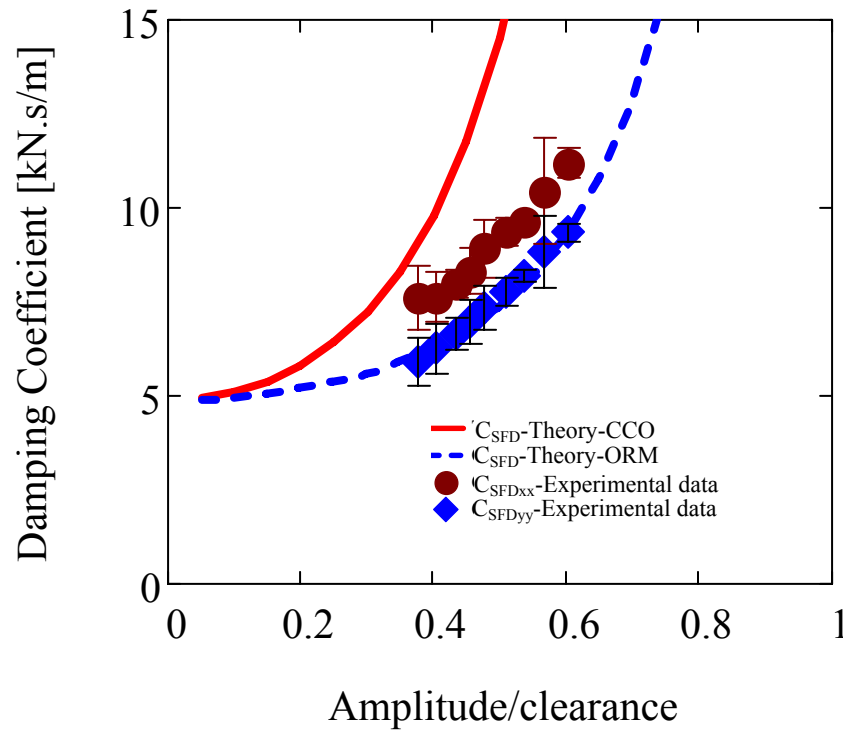
Parameter	<i>xx</i>	<i>yy</i>
System Mass, ( $M_s$ )	<b>16.3 kg</b>	<b>16.7kg</b>
Squeeze film inertia ( $M_{SFD}$ )	<b>5.9 kg</b>	<b>6.5 kg</b>
$r^2$ (goodness of curve fit)	0.97	0.97
Fluid Mass, ( $M_f$ ) [kg]	0.62	

Figure 26 and 27 show the imaginary part of the direct impedances divided by the excitation frequency, i.e.  $\text{Im}(H/\omega)$  and the identified squeeze film damping coefficients, respectively. As with the previous cases, the test derived damping coefficients are within

the predictions for CCOs and ORMs. However, the resulting coefficients are smaller and closer to the predictions for CCOs than those previously identified. These results are expected considering that the motion amplitudes exerted by the rotating force vector  $\mathbf{F}_3$  represent more circular orbital paths than purely radial motions (i.e. with  $\mathbf{F}_1$  &  $\mathbf{F}_2$ ).



**Figure 26** Imaginary part of direct impedances  $\times (1/\omega)$  versus frequency. Constant amplitude rotating load with multiple frequency sine sweep excitation.



**Figure 27 Direct squeeze film damping coefficients identified from constant amplitude rotating load with multiple frequency sine sweep excitations (Excitation vector  $F_3$ ). Predictions for circular centered orbits (CCO) and radial motion about an off-centered journal position**

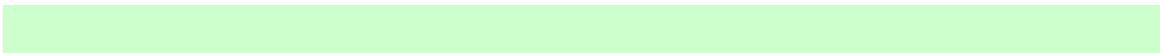
## VI Conclusions

Force coefficients of a SFD are identified while executing non-circular, multiple frequency motions. The multiple frequency excitations simulate the operation of an intershaft damper (IFD). The experiments show that the IFD damping coefficients can be obtained from system impedance functions and considering only the motion frequency component that coincides with the force excitation frequency, since this is the only component that dissipates mechanical energy. Identified cross-coupled coefficients are negligible, thus confirming the test damper operates without oil cavitation.

The forcing functions superimpose to a constant frequency excitation (25 Hz), simulating a low speed shaft, a sine sweep excitation (30 to 120 Hz) representing the excitation of a high speed shaft. The damper is excited with three types of force vectors representing either purely radial motions or circular paths due to a rotating load. The experiments include excitation with loads keeping a magnitude either constant or varying to obtain a preset bearing displacement amplitude. For the case of constant amplitude

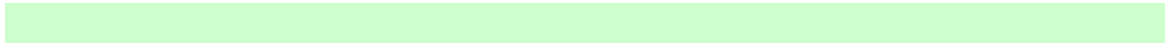
excitation force, the ensuing bearing amplitude decays steadily with frequency, and the identified viscous damping coefficients are strong functions of the amplitude of journal motion and frequency. For the case of amplitude of force increasing to maintain a certain displacement magnitude, the damping coefficients are constant within the frequency range for identification.

The experimentally obtained added mass coefficients are three times larger than those predicted by classical theory that does not include the influence of the inlet and discharge annular grooves. Predictions of added mass coefficients from an improved bulk-flow model, developed and reported in Ref.[9], are within 15% of the test values. The experimental damping coefficients are within the range of predictions derived from classical formulas for circular centered orbits or small amplitude motions about an eccentric journal position.



## VII References

- [1] Delgado, A., and San Andrés, L., 2004, “Sealed end Squeeze Film Damper: Test rig Description and Identification of Structural Parameters,” TRC report, TRC-SFD-1-04, May.
- [2] Delgado, A., and San Andrés, L., 2005, “Identification of Force Coefficients in a Squeeze Film Damper with a Mechanical Seal,” TRC report, TRC-SFD-1-05, May.
- [3] Delgado, A., and San Andrés, L., 2006, “Identification of Force Coefficients in a Squeeze Film Damper with a Mechanical Seal,” TRC report, TRC-SFD-1-06, May.
- [4] San Andrés, L., and Delgado, A., 2007, “Parameter Identification of an End Sealed SFD Part I: Identification of Force Coefficients and Operating Conditions Leading to Air Ingestion,” TRC report, TRC-SFD-1-07, May.
- [5] Hibner, D. H., 1975, “Dynamic Response of Viscous-Damped Multi-Shaft Jet Engines,” *J. Aircraft*, **12**(4), pp. 305-312
- [6] Hibner, D. H., Kirk, R. G., and Buono, D. F., 1977, “Analytical and Experimental Investigation of the Stability of Intershaft Squeeze Film Dampers,” *ASME J. Eng. Power*, **99**(1), pp. 47-52
- [7] Hibner, D. H., Bansal, P. N., and Buono, D. F., 1978, “Analysis and Experimental Investigation of the Stability of Intershaft Squeeze Film Dampers- 2: Control of Instability. *ASME J Mech. Design*, **100**(3), pp. 558-562
- [8] Gupta K., and Chatterjee S., 2007, “Dynamics of an Improved Inter Shaft Squeeze Film Damper: Theory and Experiment,” *ASME paper No. GT2007-27534*.
- [9] San Andrés, L., and Delgado, A., 2007, “Parameter Identification of an End Sealed SFD Part II: Improved Predictions of Added Mass Coefficients for Grooved SFDs and Oil Seals,” TRC report, TRC-SFD-2-06, Jun.
- [10] Chen, S., and Liu, S., 1986, “Equivalent Linearization of a Squeeze Film Damper,” *J. Vib. Acoust. Stress Reliab. Des.*, **108**(4), pp. 434-440
- [11] Della Pietra, L., and Adiletta, G., 2002, “The Squeeze Film Damper over Four Decades of Investigations. Part I: Characteristics and Operating Features,” *Shock Vib. Dig.*, **34**(1), pp. 3-26.
- [12] Della Pietra, L., and Adiletta, G., 2002, “The Squeeze Film Damper over Four Decades of Investigations. Part II: Rotordynamic Analyses with Rigid and Flexible Rotors,” *Shock Vib. Dig.*, **34**(2), pp. 97-126.
- [13] Tiwari, R., Lees A.W., Friswell, M. I., 2004, “ Identification of Dynamic Bearing Parameters: A Review,” *Shock Vib. Dig.*, **36**(2), pp. 99-124.
- [14] El-Shafei, A., Eranki, R.V., 1994, “Dynamic analysis of squeeze film damper supported rotors using equivalent linearization,” *J. Eng. Gas Turbines Power*, **116**(3), pp. 682-691.
- [15] Zhang J. X., Roberts, J.B, 1996, “A Frequency Domain Parametric Identification Method for Studying the Non-linear Performance of Squeeze Film Dampers,” *J. Sound Vib.*, **189**(2), pp. 173-191
- [16] Ellis J., Roberts, J.B, Ramli M. D., 1989, “ The Experimental Determination of Squeeze-Film Dynamic Coefficients Using the State Variable Filter Method of Parametric Identification,” *J. Tribol.*, **111**, pp. 255-2591
- [17] Diaz, S., and San Andrés, L., “A Method for Identification of Bearing Force Coefficients and Its Application to a Squeeze Film Damper with a Bubbly Lubricant,” *STLE Tribology Transactions*, Vol. 42 (4), pp. 739-746, 1999.
- [18] San Andrés, L., and De Santiago, O., 2004, “Forced Response of a Squeeze Film

- Damper and Identification of Force Coefficients from Large Orbital Motions,” ASME Journal of Tribology, **126**(2), pp. 292-300
- [19] Zeidan, F.Y., San Andrés, L., and Vance, J. M., 1996, “Design and Application of Squeeze Film Dampers in Rotating Machinery,” *Proc. 25<sup>th</sup> Turbomachinery Symposium*, Houston, TX, pp.169-188.
- [20] San Andrés, 1985, “Effect of Fluid Inertia Effect on Squeeze Film Damper Force Response,” Ph.D. Dissertation, December, Texas A&M University, College Station, TX.
- [21] Rodriguez, L. E., 2004, “Experimental Frequency-Dependent Rotordynamic Coefficients For a Load-On-Pad, High-Speed, Flexible-Pivot Tilting Pad Bearing,” M.S. Thesis, Texas A&M University, College Station, TX.
- 

## Appendix A Identification of Structural Parameters (dry system tests)

The static and impact tests stand to verify the stiffness, mass and damping coefficient of the test damper and structure prior to the identification of the force parameter of the squeeze film alone. Figure A1 shows the results from the static tests using a strain gauge load cell and readings from the eddy current sensors. Table A 1 shows the identified coefficients. The coefficients are within the uncertainty of the ones previously identified, see Ref. [3]  $K_{sx}=853$  kN/m,  $K_{sy}=885$  kN/m.

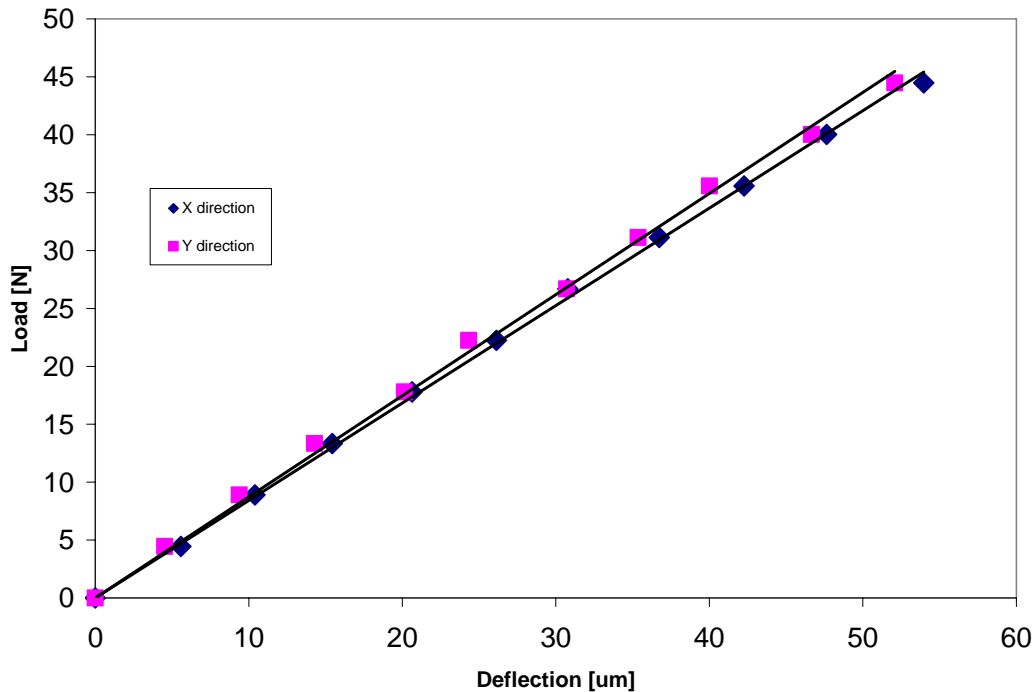


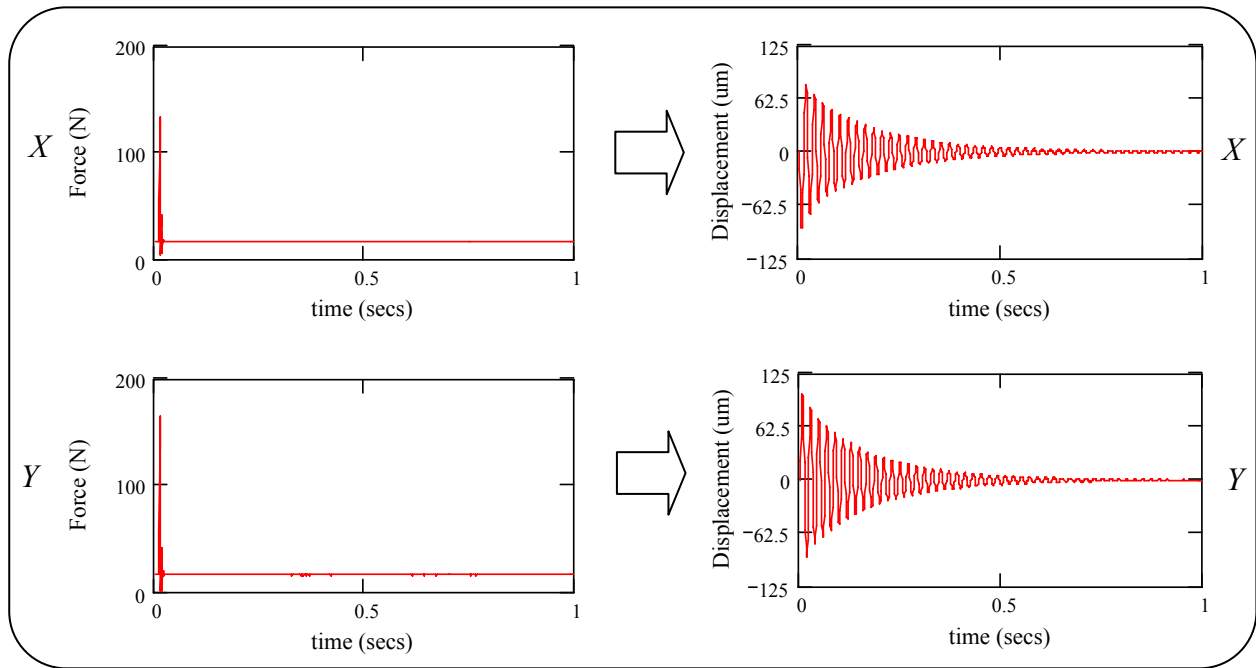
Figure A 1 Bearing deflection versus static load (X,Y directions)

Table A 1 Structural stiffnesses of support from static load tests

	$K_{sx}$ [N/m]	$K_{sy}$ [N/m]
Value	$840 \times 10^3$	$865 \times 10^3$
Uncertainty	$25 \times 10^3$ [~3%]	$26 \times 10^3$ [~3%]
Range[N]	0 to 50	0 to 50

Figure A2 shows a typical impact load and bearing displacement responses in the  $x$  and  $y$  directions. Figures A3 and A4 show the system transfer functions in the  $X$  and  $Y$  directions obtained from the impact test (10 averages), respectively. Table A 2 presents the results from the impact tests exerted on the bearing assembly. Again, the results are

consistent with values reported in Ref [3]. Notice in Fig. A3 and A4 that the curve fit reproduces well the experimental data at the frequencies close to zero, which is important to obtain accurate stiffness coefficient (i.e. similar to that obtained from static tests).



**Figure A 2 Impact load and displacements (X, Y) versus time (dry system)**

**Table A 2 Identified parameters from impact tests exerted on SFD test section (no lubricant)**

Parameters	<i>X</i>	<i>Y</i>
Stiffness, $K_s$ [kN/m]	863 ( $\pm 43$ )	906 ( $\pm 45$ )
SI Mass, $M$ [kg]	9.5 ( $\pm 0.5$ )	9.3 ( $\pm 0.5$ )
Damping, $C_s$ [N.s/m]	124	125
Damping ratio, $\zeta$	0.019	0.022
Natural Frequency $f_n$ [Hz]	48 $\pm$ 1	50 $\pm$ 1
$R^2$ (goodness of fit)	0.99	0.99

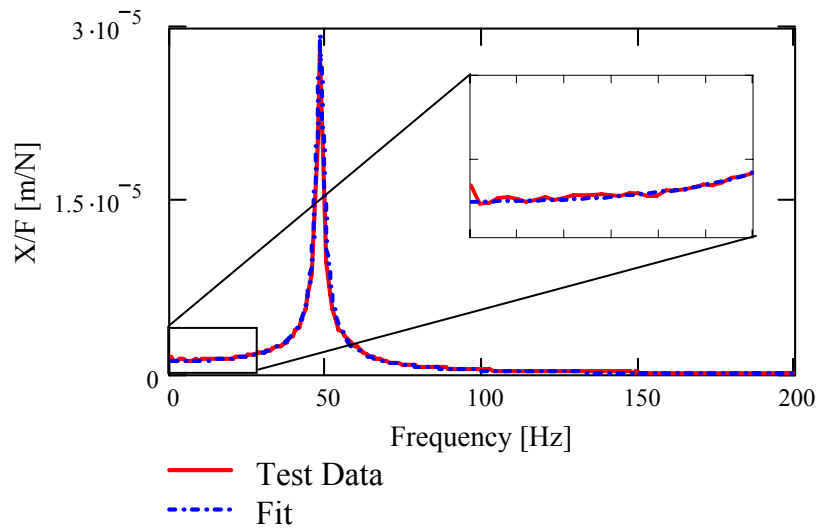


**Figure A 3 Transfer function ( $X/F_x$ ) from impact load tests and curve fit for motions along X direction. (Dry system, no seal)**

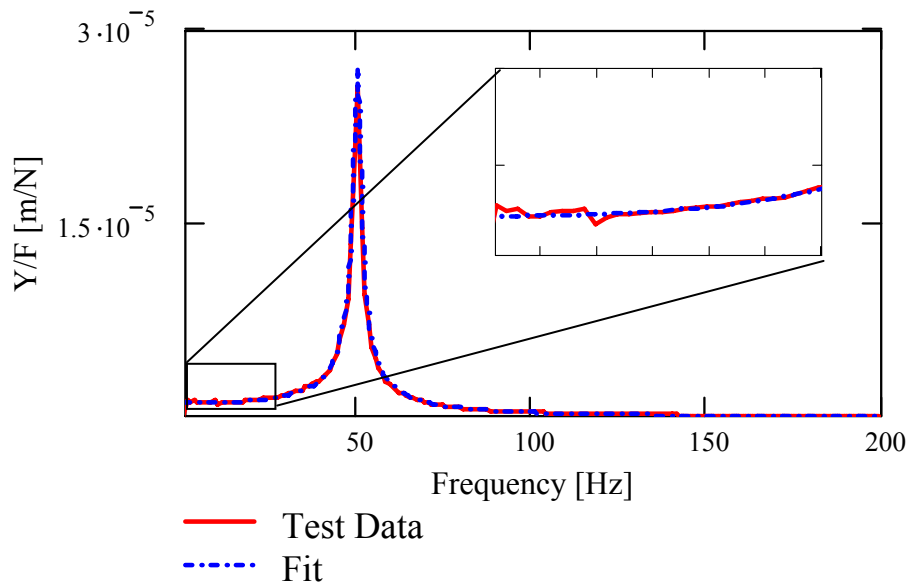


**Figure A 4 Transfer function ( $Y/F_y$ ) from impact load tests and curve fit for motions along Y direction. (Dry system, no seal)**

## Appendix B Cross-coupled Impedance Functions Identified From Multiple Frequency Sine Sweep Excitation with Constant Amplitude

The appendix presents the cross-coupled impedance functions resulting from the identification procedure using sine sweep excitation with constant load amplitude (i.e. forcing vectors  $F_1$  and  $F_2$ ). Figures B1 and B2 show the real and imaginary part of the cross-coupled impedance functions, respectively. The results indicate that the cross coupled coefficients are negligible within the frequency range for identification. Table B1 presents the identified force coefficients. Note that the cross-coupled coefficients are of the same order of magnitude as the uncertainty associated to the identified direct coefficients. Furthermore, the cross impedance functions are relatively constant and close to zero. Thus, regardless of the physical model used to curve fit, the correlation values are expected to be small.

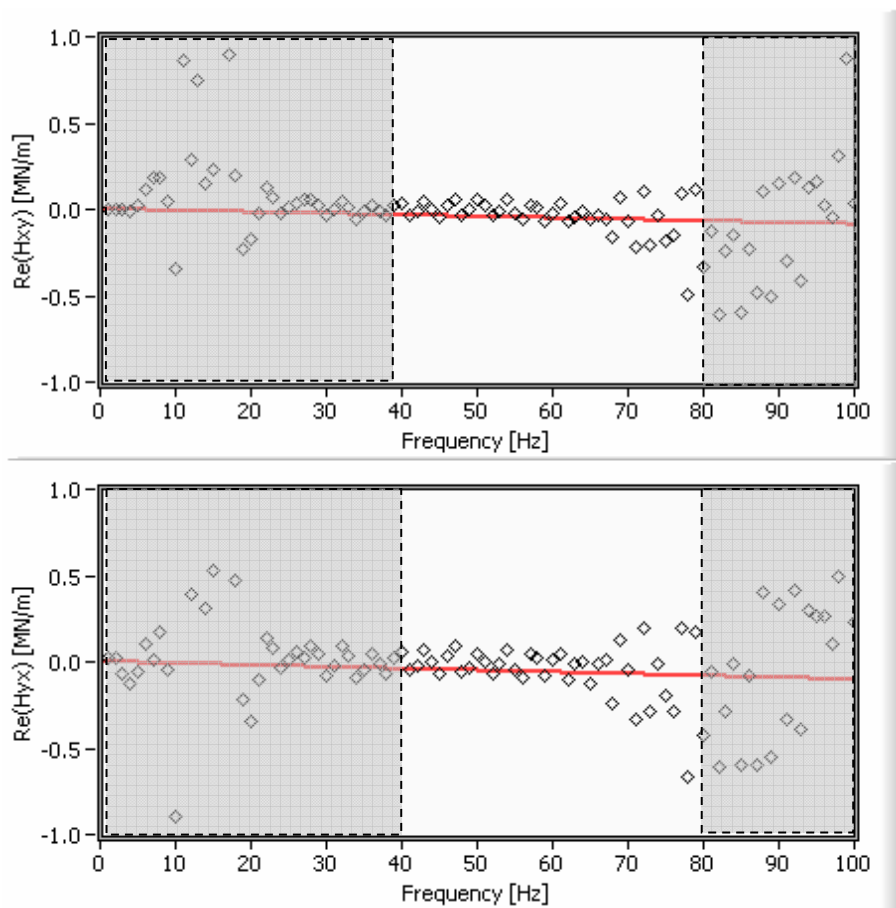


**Figure B 1 Real part of cross-coupled impedances versus frequency. Multiple frequency excitation (constant 25 Hz + sine sweep 30-120 Hz). Excitation vectors  $F_1$  &  $F_2$**

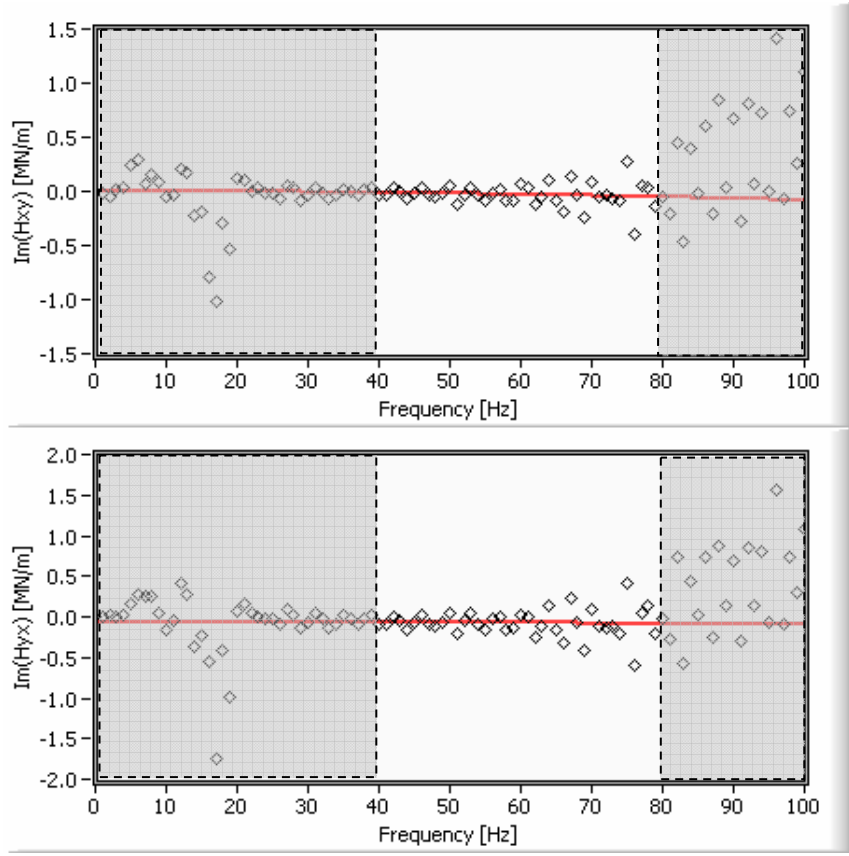


**Figure B 2 Imaginary part of cross-coupled impedances versus frequency. Multiple frequency excitation (constant 25 Hz + sine sweep 30-120 Hz). Excitation vectors  $F_1$  &  $F_2$**

**Table B 1 Identified cross-coupled coefficients from constant amplitude load & sine sweep excitation tests**

$K_{xy}$	$M_{xy}$	$K_{yx}$	$M_{yx}$	$C_{xy}$	$C_{yx}$
[N/m]	[kg]	[N/m]	[kg]	[N.s/m]	[N.s/m]
-1445	0.1	-61220	0.2	-140	-170
$r^2=0.21$		$r^2=0.19$		$r^2=0.18$	$r^2=0.19$